Earth-Science Reviews 208 (2020) 103254

Contents lists available at ScienceDirect

Earth-Science Reviews

journal homepage: www.elsevier.com/locate/earscirev

Two-phased collapse of the shallow-water carbonate factory during the late Pliensbachian–Toarcian driven by changing climate and enhanced continental weathering in the Northwestern Gondwana Margin

Francois-Nicolas Krencker[a,*], Alicia Fantasia[a], Jan Danisch[a], Rowan Martindale[b], Lahcen Kabiri[c], Mohamed El Ouali[c], Stéphane Bodin[a]

[a] Department of Geoscience, Aarhus University, Høegh-Guldbergs Gade 2, 8000 Aarhus C, Denmark
[b] Department of Geological Sciences, The University of Texas at Austin, 2275 Speedway Stop C9000, Austin, TX 78712, USA
[c] Sciences and Techniques Faculty of Errachidia, Department of Geoscience, Moulay Ismail University, BP 509, Boutalamine-Errachidia, Morocco

ARTICLE INFO

Keywords:
Early Jurassic
Carbonate factory shutdown
Oceanic Anoxic Event
Tethys Ocean
Morocco

ABSTRACT

The end Pliensbachian–Toarcian is characterized by several carbon-cycle perturbations and faunal turnovers (e.g., ammonites and foraminifera), which are most likely triggered by pulses of the Karoo-Ferrar-Chon Aike large igneous province. The majority of information about these events is based on detailed studies of sites deposited in deep-water settings, which leaves vast uncertainties about the expression of, and response to, these events in shallow-marine ecosystems. Here, we present a comprehensive assessment of paleoclimatic impacts on neritic depositional environments from the latest Pliensbachian through the middle Toarcian in the central High Atlas Basin, Morocco, and compare those with changes observed in coeval neritic environments within the western Tethyan realm. A total of four new stratigraphic sections were investigated in the southern part of central High Atlas Basin and these new sections are synthesized with six previously published sections, distributed over eight localities. Correlations between sections are based on biostratigraphy, chemostratigraphy and lithostratigraphy. In Morocco, two episodes of carbonate factory shutdown are observed, spanning the Pliensbachian/Toarcian boundary and the Polymorphum/Levisoni transition. Each carbonate factory collapse correlates to well-documented environmental disturbances during the latest Pliensbachian–middle Toarcian interval, including the Toarcian Oceanic Anoxic Event (T-OAE). Moreover, each episode of carbonate factory shutdown coincides with an interval characterized by a significant increase of coarse siliciclastic input in the basin, further demonstrating the link between global warming, increased continental weathering, and ecosystem turnovers. Furthermore, these two episodes of carbonate factory shutdown are each followed by episodes of renewed carbonate production, showing the resilience of the neritic carbonate factory in this region. The first recovery interval, occurring during the late Polymorphum Zone, is associated with a mixed siliciclastic-carbonate system. The second episode of carbonate recovery quickly follows the shutdown associated with the onset of the T-OAE. It is associated with an abiotic-dominated carbonate production mode, resulting in an elevated ooid production. A full recovery of biotic carbonate production only occurs in the late stage of the T-OAE. Although biotic turnover occurs at both events, from a shallow-marine perspective, the major biotic and abiotic crisis occurred at the Pliensbachian/Toarcian boundary and not during the T-OAE. This is in contrast to the deep-marine record, where the T-OAE is often inferred to be the most significant event. An enhanced hydrological cycle and the subsequent increase of continental nutrient shedding might have triggered the most severe changes of the carbonate productivity at the Pliensbachian/Toarcian transition; whereas, ocean acidification and increased storm activity likely played a significant role at the onset of the T-OAE.

1. Introduction

The late Pliensbachian–Toarcian was punctuated by intense environmental disturbances leading to several global turnovers in marine invertebrate fauna, occurring at: i) the Pliensbachian/Toarcian boundary, ii) the early Toarcian Polymorphum–Levisoni ammonite

* Corresponding author.
E-mail address: fkrencker@geo.au.dk (F.-N. Krencker).

https://doi.org/10.1016/j.earscirev.2020.103254
Received 10 April 2020; Received in revised form 11 June 2020; Accepted 13 June 2020
Available online 29 June 2020

Zones transition, iii) the middle–upper Toarcian transition, and iv) the late Toarcian Dispansum Zone (e.g., Little and Benton, 1995; Harries and Little, 1999; Cecca and Macchioni, 2004; Mattioli and Pittet, 2004; Mattioli et al., 2008, 2009; Dera et al., 2010; Suan et al., 2010; Caruthers et al., 2013, 2014; Martindale and Aberhan, 2017). Although the precise causes of these biotic crises are still debated, the prevailing hypothesis is that they are related to extreme oceanic temperature fluctuations (Gomez et al., 2008; Suan et al., 2010; Dera et al., 2011a; Krencker et al., 2014), oceanic oxygenation deficiency (Wignall et al., 2005; Jenkyns, 2010; Montero-Serrano et al., 2015; Martindale and Aberhan, 2017; Them et al., 2018), change of the oceanic nutrient levels due to enhanced continental weathering (Cohen et al., 2004; Bodin et al., 2010; Brazier et al., 2015; Montero-Serrano et al., 2015; Percival et al., 2016; Them et al., 2017b; Fantasia et al., 2018b), or ocean acidification (Suan et al., 2008; Trecalli et al., 2012; Ettinger et al., 2020). Among these events, the early Toarcian Polymorphum–Levisoni environmental changes are considered to be the most severe as they were associated with a drastic warming in tropical and subtropical seawater temperatures (McArthur et al., 2000; Gomez et al., 2008; Dera et al., 2009a; Suan et al., 2010; Ullmann et al., 2020). In Europe, the lowermost Falciferum (Levisoni equivalent) interval in the early Toarcian is associated with organic-rich horizons linked to de-oxygenated waters and is often referred to as the Toarcian Oceanic Anoxic Event (T-OAE; Jenkyns, 1988, 2010). The T-OAE is characterized by a negative carbon isotope excursion recorded worldwide in bulk marine carbonate micrite and organic matter, wood debris, brachiopod shells, and biomarkers (Hesselbo et al., 2000; 2007; Al-Suwaidi et al., 2010; Caruthers et al., 2011; Gröcke et al., 2011; Guex et al., 2012; French et al., 2014; Ullmann et al., 2014, 2020; Bodin et al., 2016; Suan et al., 2016; Them et al., 2017a; Fantasia et al., 2018a; Ruebsam et al., 2020b).

Carbonate platforms were affected by the environmental changes occurring at the Pliensbachian/Toarcian boundary (Cope et al., 1980; Dromart et al., 1996; Röhl et al., 2001; Hesselbo et al., 2007; Suan et al., 2008; Trecalli et al., 2012; Han et al., 2018), commonly referred to as the Pl/To event. The exact geochemical characterization of the Pl/To event is still a work in progress. Indeed, in England and Portugal this event is associated with a negative carbon isotope excursion (Hesselbo et al., 2007; Littler et al., 2010). A carbon isotope excursion at the Pliensbachian/Toarcian boundary is also well expressed in the northern Paris Basin (Ruebsam et al., 2019) and possibly in the Sancerre Core (e.g. Hermoso et al., 2013). In Morocco (Bodin et al., 2016) and Chile (Fantasia et al., 2018a), the Pliensbachian/Toarcian transition is, however, characterized by a 3–4‰ positive carbon isotope shifts recorded in the organic carbon phase. The lack of agreement between isotopic patterns from different basins around the globe likely indicates that the Pl/To and T-OAE events represent different scenarios of environmental perturbation (Bodin et al., 2016; see also the review on the Toarcian carbon isotope stratigraphy in Ruebsam and Al-Husseini, 2020). Alternatively, the disagreement could be an artifact related to the strong sedimentological condensation associated with the Pliensbachian/Toarcian transition in European sections. Nonetheless, volcanic activity of the Karoo-Ferrar-Chon Aike large igneous province is commonly invoked to explain the broad range of environmental disturbances that occurred during the time interval associated with both the Pl/To and the T-OAE. This hypothesis is based on the concomitance of the main magmatic pulses of the Karoo-Ferrar-Chon Aike and the timing of the Toarcian faunal turnovers (Svensen et al., 2007; Jourdan et al., 2008; Suan et al., 2008; Dera et al., 2010; Caruthers et al., 2013; Svensen et al., 2018), as well as the presence of mercury (Hg) anomalies in the stratigraphic record within the T-OAE stratigraphic interval thought to be the signature of enhanced volcanic activity (Percival et al., 2015, 2016).

Despite the significance of these Pliensbachian–Toarcian events, most studies, to date, have focused on pelagic and hemipelagic settings and organic-rich rocks leaving a large knowledge gap about how shallow-water carbonate ecosystems responded. Carbonate productivity is an important factor in understanding these carbon cycle perturbations, as it is relevant to the Jurassic exogenic carbon-cycle given the very weak pelagic carbonate production during this time interval (e.g. Eichenseer et al., 2019; Suchéras-Marx et al., 2019). In this study, we investigate the temporal and spatial evolution of the carbonate productivity in the central High Atlas within the uppermost Pliensbachian–Toarcian interval. Interpretations are based on the detailed description of four new stratigraphic sections, complementing the published dataset of Krencker et al. (2014, 2015, 2019) and Bodin et al. (2010, 2011, 2016), see also reference list in supplementary data 1). This large dataset is then used to characterize the spatio-temporal organization of sedimentary facies along the northern Gondwana continental shelf. The chronostratigraphy of the studied sections is based on integrated biostratigraphy and carbon isotope chemostratigraphy. The main outcomes of this study are discussed within the current knowledge of the Pliensbachian–Toarcian global environmental disturbances.

2. Geotectonic setting

The central High Atlas Basin developed during two extensional phases occurring during the Middle–Late Triassic and Early Jurassic (late Sinemurian and Pliensbachian) (Frizon de Lamotte et al., 2008; Wilmsen and Neuweiler, 2008; Lachkar et al., 2009; Moragas et al., 2018). It is characterized by primary NE–SW and subordinate NW–SE folds affecting Early–Middle Jurassic strata. Present-day configuration and uplift are related to the Cenozoic convergence between Africa and Eurasia (Teixell et al., 2003; Laville et al., 2004; Frizon de Lamotte et al., 2008). During the Pliensbachian–Toarcian, the central High Atlas Basin was located at the northern margin of Gondwana, in a tropical paleolatitude, and opened to the Tethys to the east (Fig. 1A; Scotese, 2016). Sedimentation was dominated by biogenic carbonate deposits interrupted twice by siliciclastic pulses during the early and the late Toarcian, which are interpreted to reflect climatic changes from dry to more humid conditions (Wilmsen and Neuweiler, 2008; Bodin et al., 2010, 2016; Krencker et al., 2014).

3. Materials and methods

3.1. Field approach and petrography

In the central High Atlas, 4 sections were measured in 3 areas: i) the Dades Valley; ii) close to the village of Aghbalou N'Kerdous; and iii) the NW part of the High Atlas, approximately 30 km SE of Beni Mellal (Fig. 1B). A total of 840 m of upper Pliensbachian–Toarcian sedimentary rocks were logged and described bed by bed. The focus was on lateral and stratigraphic facies change, sedimentary features and textures, biota, trace fossils and diagenetic features. Correlations between sections are based on biostratigraphy, chemostratigraphy, and lithostratigraphy. For sections located close to each other, direct visual correlation coupled with satellite imagery was used. GPS coordinates of measured sections are presented in Table 1. Facies table and colour-coding for outcrop sections are given in Table 2.

3.2. Bulk micrite geochemical analyzes

A total of 211 bulk micrite samples from the upper Pliensbachian–Toarcian were collected at Aghbalou N'Kerdous, Ouguerd Zegzaoune, Taguendouft, and Tamtetoucht with an average sample spacing of 2 m. For each horizon, about 2 mg of the micritic part of non-weathered mudstone and marlstone samples lacking allochems and diagenetic veins were selected and then ground to powder and homogenized using an agate mortar. Ground samples were treated two times with 6 M HCl for 12 h to remove any carbonate phases and rinsed subsequently with deionized H_2O until neutrality was reached. The total organic carbon isotope ratios ($\delta^{13}C_{TOC}$) in decarbonated samples

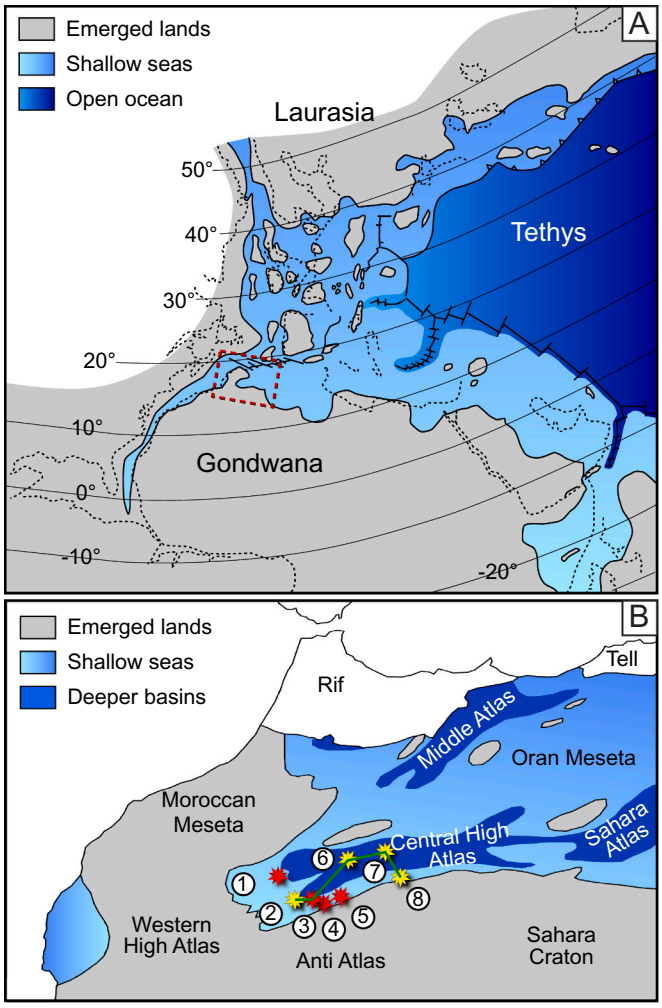

Fig. 1. Toarcian paleogeographic map. A: Western Tethyan realm (Bassoulet et al., 1993) indicating the approximate position of the studied area with a dashed rectangle. B: Paleogeographic map of Morocco and western Algeria showing major geological provinces (modified from Du Dresnay, 1971; and Blomeier and Reijmer, 1999) and the location of the sections discussed in this study: 1) Taguendouft, 2) Boumardoul n'Imazighn, 3) Ouguerd Zegzaoune, 4) Tamtetoucht, 5) Aghbalou N'Kerdous, 6) Amellago, 7) Foum Tillicht, and 8) Ait Athmane. Red stars represent newly described sections (this study) and yellow stars represent previously published sections (Bodin et al., 2010, 2011, 2016; Krencker et al., 2014, 2015, 2019). The green line corresponds to the chronostratigraphic chart position. (For interpretation of the references to colour in this figure legend, the reader is referred to the web version of this article.)

Table 1
GPS coordinates of the studied sections.

Section names	Latitudes	Longitudes
Aghbalou N'Kerdous	31,766,389	−5,305,167
Tamtetoucht	31,657,183	−5,571,967
Ouguerd Zegzaoune	31,079867	−5,741,869
Taguendouft	32,079867	−6,275,427

were determined using a Flash EA 2000 elemental analyzer connected online to ThermoFinnigan Delta V Plus mass spectrometer at the university of Erlangen-Nuremberg. All carbon isotope values are reported in the conventional δ-notation in permil relative to V-PDB (Vienna PeeDee Belemnite). Accuracy and reproducibility of the analyzes were checked by replicate analyzes of laboratory standards calibrated to international standards USGS 40 and 41. Reproducibility was ± 0.06‰ (1σ).

4. Lithostratigraphy and biostratigraphy of the central High Atlas

In the central High Atlas, the upper Pliensbachian–Toarcian interval is subdivided into nine lithostratigraphic formations. For the upper Pliensbachian, four formations are recognized: the Aganane Formation (Septfontaine, 1985), the Choucht Formation (Septfontaine, 1985),

the Aberdouz Formation (Stüder and du Dresnay, 1980), and the Ouchbis Formation (Stüder and du Dresnay, 1980). The Toarcian formations are: the Tagoudite Formation (Stüder and du Dresnay, 1980), the Wazzant/Azilal Formation (Jossen, 1988; Ettaki et al., 2000), the Tafraout Formation (Bouchouata et al., 1995), the Ait Athmane Formation (Wilmsen et al., 2002), and the Agoudim 1 Formation (Stüder and du Dresnay, 1980). Age assignments of these formations are schematically reported in Fig. 2 and extensively described, together with their lithological characteristics, in the supplementary data SD1.

5. Data reporting and interpretation

Within the central High Atlas Basin, 4 new stratigraphic sections were investigated: Aghbalou N'Kerdous, Ouguerd Zegzaoune, Taguendouft, and Tamtetoucht (Fig. 3). These sections, distributed along the southern, western, and northwestern part of the basin, complement previously published data from the Amellago, Ait Athmane, Bou Oumardoul, Jebel Toksine, Foum Tillicht, and Jebel Akenzoud sections (Fig. 1; Wilmsen et al., 2002; Wilmsen and Neuweiler, 2008; Bodin et al., 2010, 2016; Krencker et al., 2014, 2015, 2019; Martinez et al., 2017; Brame et al., 2019). Altogether, these sites offer extended paleogeographical coverage of the central High Atlas and bring together a coherent picture of changes in carbonate factory and siliciclastic supply during the late Early Jurassic. This section describes the stratigraphy and temporal constraints of the four new sections in detail.

5.1. Aghbalou N'Kerdous

5.1.1. Stratigraphy

The Aghbalou N'Kerdous section (Fig. 3) is approximately 160 m thick and is located in the vicinity of the village with the same name (Table 1). The first 20 m of the section corresponds to alternations of red lagoonal calcareous siltstones (Fig. 4A) and limestone beds with microbial crenulations belonging to the Aganane Formation (Aghbalou 3 Formation from Hadri, 1997). The red fissile claystone intervals are silt-rich and include evaporites (e.g., gypsum). The limestone laminations are planar, wavy, and crenulated and are interpreted to be microbial in origin. No macroscopic fossils have been observed within this interval. At approximately 20 m in the section, a 4-m-thick lithiotid framestone bed (Fig.4B) is observed and is capped by approximately 6 m of predominantly oncoid-rich grainstones to rudstones (Fig. 4C) and peloid-rich grainstones (Fig. 4D, E) showing similar facies as the Aganane Formation at the Ait Athmane section (Krencker et al., 2014). The Pliensbachian/Toarcian transition is recorded within an approximately 10-m-thick fissile interval overlaid by a 10-m-thick ooid and bioclast-rich grainstones (Fig. 4F) and a 3-m-thick lithiotid framestone belonging to the Tafraout Formation. From 50 to 70 m, a fissile red silt-rich unfossiliferous claystone interval is documented. This interval includes numerous silt beds interpreted as storm deposits progressively replaced by ooid-rich grainstones. The interval between 80 m and 118 m is dominated by a carbonate-rich marlstone interval including numerous 2-m-thick packstone to grainstone beds including a diversified fauna (e.g., crinoids, brachiopods, bivalves, and gastropods) and ooids. At 110 m, a 1-m-thick dissolution horizon is observed; it is filled with a monomictite conglomerate including angular carbonate intraclasts. The top 10 m of the Tafraout Formation in Aghbalou N'Kerdous corresponds to a coral framestone. Other allochems include crinoid ossicles, oncoids, brachiopods, and bivalves (Fig. 4G), which are indicative of normal marine salinity and oxygenated conditions. The last 30 m of the section corresponds to versicolor claystones

Table 2
Overview of facies classification and interpretation.

Color Code	Sedimentary Facies	Texture	Allochems	Descritption	Depositional Environment
1a	Polymictic conglomerate extraclast-rich	g, vcs, cs, ms	Extraclast (diverse metamorphic rocks, quartz, feldspar) [4], glauconite [2]	Angular to sub-angular extraclasts	Continental, river-dominated
1b	Polymictic conglomerate intraclast-rich	g, vcs, cs, ms	Intraclast [4], glauconite [2]	Rounded to sub-rounded intraclasts	Paralic, tide-dominated
1c	Paralic claystone and laminated facies	cly, M–W, B	Peloid [2], plant debris [2], lithoclast (quartz, glauconite) [2]	Presence of microbial mat, paleosoils	Tidal mudflat, schorre
1d	Peloid-rich facies	F, G, P, M, m	Peloid [4], foraminifera [2], bioclast [1–2], lithoclast (quartz, glauconite, intraclast) [1–2], oncoids [1–4]	Massive beds, *Cayeuxia, Thaumatoporella*, *Arenicolites*, diagenetic mudstone	Shallow-sub-tidal (inner platform)
1e	Ooid-rich facies	G, P	Ooid [4], bioclast [1–2], lithoclast (some quartz, glauconite) [1–2], peloid [1–2]	Tidalites, flaser bedding, wave ripples, trough cross-bedding	Tidal sandflat (inner platform)
1f	Cross-stratified sandstone	vcs, cs, ms	Extraclast (diverse metamorphic rocks, quartz, feldspar) [4], plant debris [1], bioclast [2–3]	Wave ripples, trough cross-bedding, common shell lags on foresets	Shoreface (inner platform)
2a	Coral-microbial bioherms	B, R, F	Hermatypic coral [4], microbialite [4]	Framestone, slightly transported bioclasts, trace of microbial bioturbation	Open marine (inner–middle platform)
2b	Bivalve (lithiotid) biostromes / bioherms	B, R, F	Bivalve (lithiotid) [4], gastropod [2], solitary coral [2], brachiopod [2], bioclast [3], peloid [3], ooid [1–2]	Bouquet-like bioconstruction, slightly transported bioclasts	Open marine (inner–middle platform)
2c	Diverse fauna facies	F, W–P, P, m	Echinoderms [2–3], bivalve [2–3], gastropod [2–3], brachiopod [2], ammonite [2], bioclast [3], lithoclast (incl. quartz) [2–3]	Metric marlstone intervals incised by P, W–P beds, cross-bedding	Open marine (proximal middle platform)
2d	Hummocky cross stratification	fs, slt minor: ms	Lithoclast (incl. quartz, glauconite) [4], plant debris [1], bioclast [1–2]	Hummocky cross stratification	Open marine, storm dominated (inner–mid-dle platform)
2e	Isolated coarse to fine-grained storm deposits	fs, slt, cly	Lithoclast (incl. quartz) [4], plant debris [2]	Wavy stratification	Open marine, storm dominated (inner–mid-dle platfrom)
3a	Marly facies	m, M,M–W minor: W, P	Ammonite [2], belemnite [2], echinoderm [2], oyster [2], gastropod [1–2], foraminifera [1–2], lithoclasts (some quartz) [0–2], ostracod [1–2]	Limestone/marlstone alternations, *Zoophycos*, *Diplocraterion*, *Arenicolites*, *Thalassinoides*, *Chondrites*	Hemipelagic (outer platform)
3b	Slumps, Turbidites	fs, slt, cly	Lithoclast (incl. quartz) [1], intraclast [1], plant debris [2], wood debris [2], bioclast [2], ammonite [0–2], ophiure [0–1]	Turbidite sequences, flute casts, groove marks, linguoide ripples	Hemipelagic (proximal outer platform)
3c	Argillaceous facies	slt, cly	Lithoclast (incl. quartz) [4], plant debris [2–3], wood debris [2–3], bioclast [1–2], ammonite [0–1], foraminifera [0–1]	Claystone-dominated facies rarely interrupted by siltstone beds	Hemipelagic (distal outer platform)

Numbers indicate the relative abundance of allochems: 0 = absent, 1 = present, 2 = frequent, 3 = abundant, 4 = dominant. For carbonate rock texture: m = marls, M = mudstone, W = wackestone, P = packstone, G = grainstone, F = floatstone, R = rudstone, B = boundstone. For siliciclastic rock texture: cly = claystone, slt = siltstone, fs = fine sandstone, ms = medium sandstone, cs = coarse sandstone, vcs = very coarse sandstone, g = gravel.

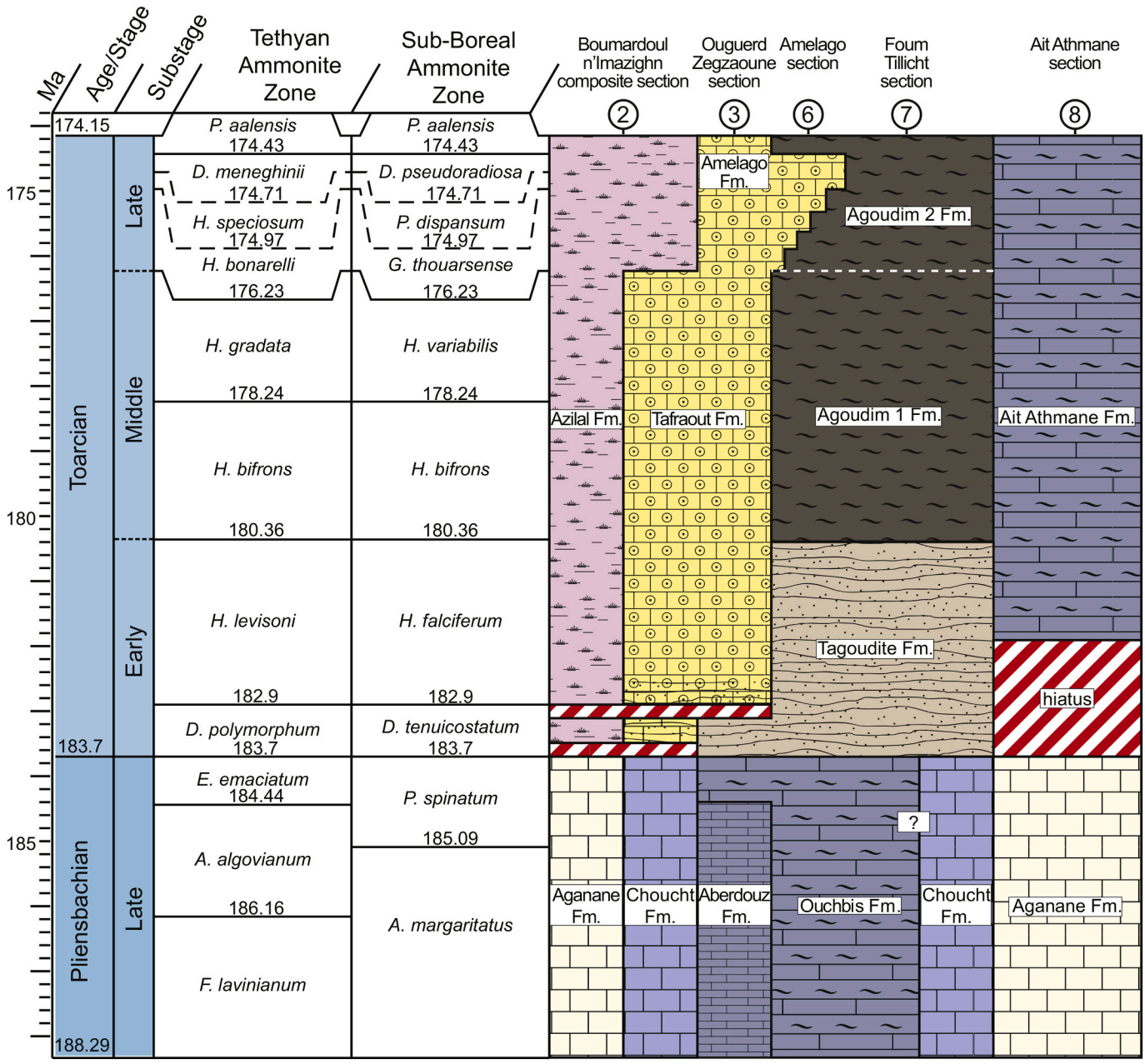

Fig. 2. Late Pliensbachian–Aalenian chronostratigraphic chart for the central High Atlas (based upon Ibouh et al., 2001; Wilmsen et al., 2002; Mehdi et al., 2003; Ettaki and Chellaï, 2005; Wilmsen and Neuweiler, 2008; Bodin et al., 2010, 2011, 2016; Krencker et al., 2014, 2015, 2019; this study). The chronostratigraphic chart position is indicated on Fig. 1B. with a green line. Red hatched areas represent stratigraphic gaps (unconformities); Figure produced with TSCreator (https://engineering.purdue.edu/Stratigraphy/tscreator). All ages on the timeline are in Ma (Ogg et al., 2016). (For interpretation of the references to colour in this figure legend, the reader is referred to the web version of this article.)

interfingered with centimeter to meter-scale beds of dolomitized mudstones, dolomitized peloidal packstones, and dolomitized ooid grainstones (Fig. 4H) belonging to the Azilal Formation.

5.1.2. Chronostratigraphic framework

Thirty-one samples were collected at the Aghbalou N'Kerdous section between 29 m and 101.5 m to analyze their total organic carbon isotope composition (Fig. 3). The carbon isotope profile can be divided into three intervals. Interval 1 (29–43 m) is characterized by highly fluctuating $\delta^{13}C_{org}$ values with minimum and maximum values of −26.7‰ and − 23.5‰, respectively. Interval 2 (40–89.5 m) records a 4‰ negative carbon isotope excursion with pre- and post-excursion values of −23.8‰ and a minimum value of −27.8‰. Interval 3 (89.5–101.5 m) is characterized by $\delta^{13}C_{org}$ values oscillating around −24‰ with minimum and maximum values of −24.8‰ and − 23.2‰. Several brachiopods have been collected at the Aghbalou N'Kerdous section (Fig. 3).

The occurrence of *Liospiriferina undulata* at 42 m indicates that this level was deposited before the Polymorphum/Levisoni boundary (Baeza-Carratalá et al., 2011). Within the same bed, *Zeilleria culeiformis* likely indicates a late Pliensbachian–early Toarcian age, as *Z. culeiformis* is often found in uppermost Pliensbachian–lowermost Toarcian strata in NW Europe (Rengifo et al., 2015). Interval 2 (40–89.5 m) characterized by the 4‰ negative carbon isotope excursion is also associated with red storm deposits located just above the horizons where brachiopods have been collected. Interval 2 is, therefore, correlated to the T-OAE stratigraphic interval based on biostratigraphy and chemostratigraphy, as well as the common and ubiquitous occurrence of storm deposits in

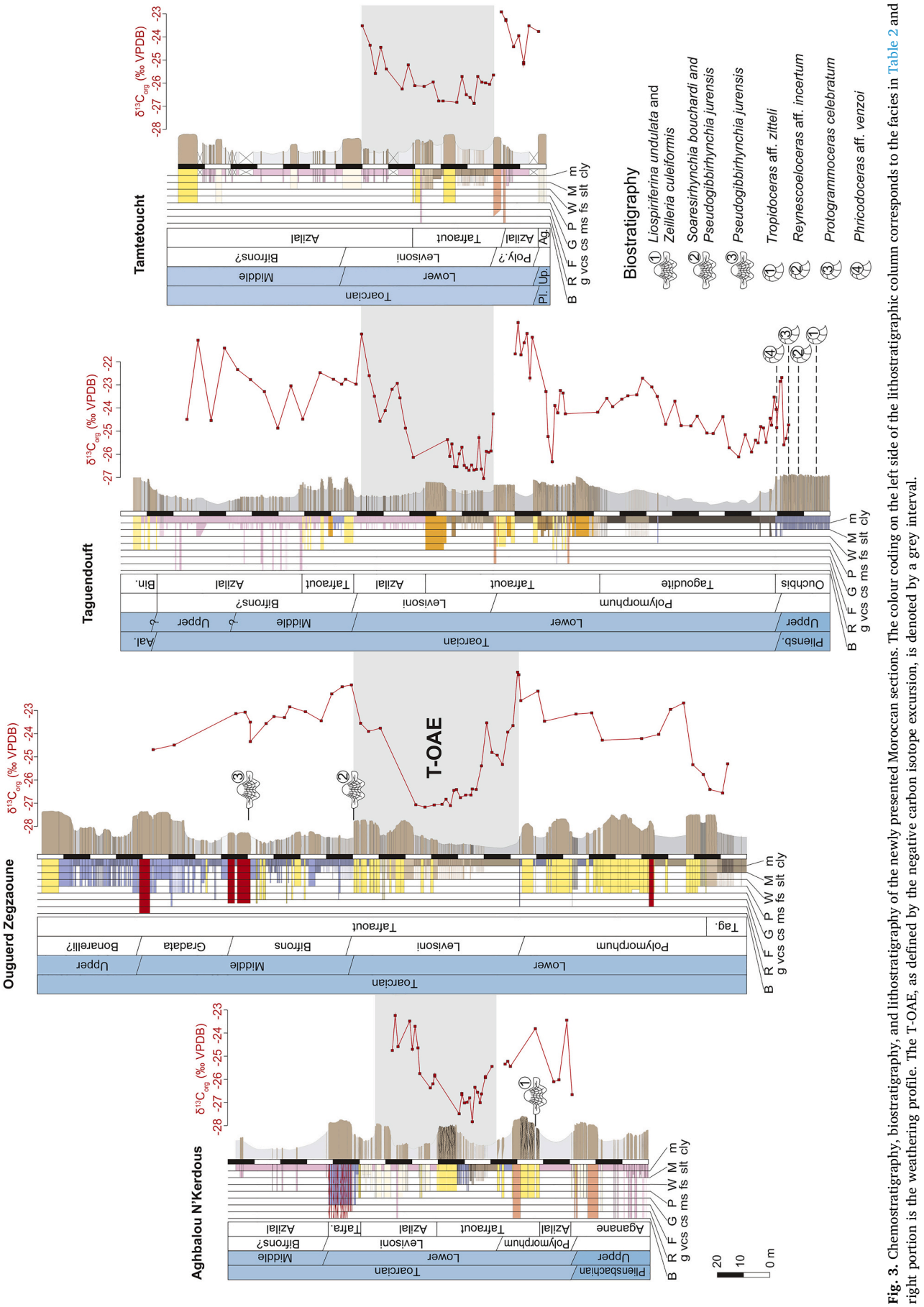

Fig. 3. Chemostratigraphy, biostratigraphy, and lithostratigraphy of the newly presented Moroccan sections. The colour coding on the left side of the lithostratigraphic column corresponds to the facies in Table 2 and the right portion is the weathering profile. The T-OAE, as defined by the negative carbon isotope excursion, is denoted by a grey interval.

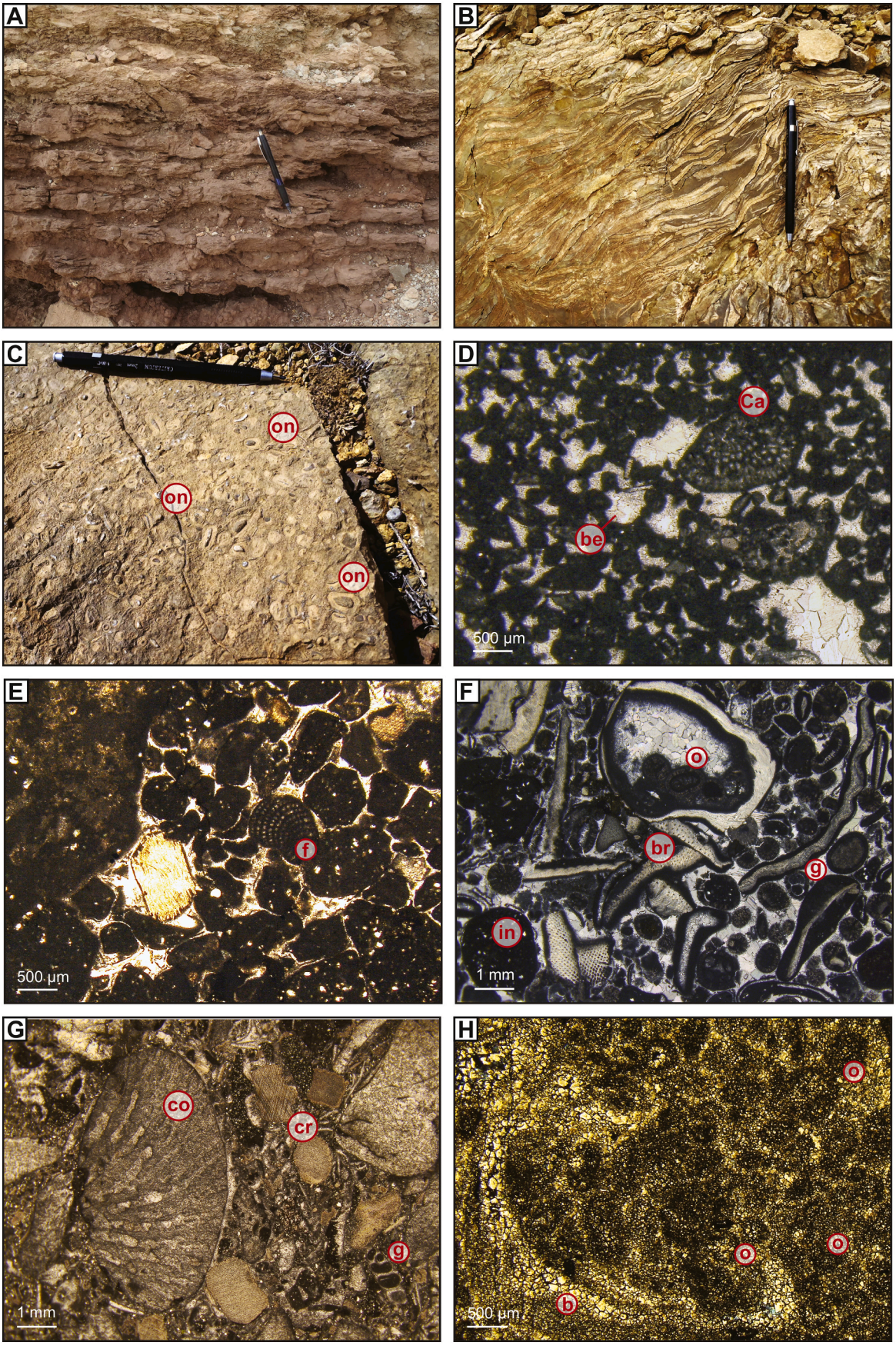

(caption on next page)

Fig. 4. Outcrop photographs and photomicrographs of upper Pliensbachian lithostratigraphic formations; pencil (10 cm), or rock hammer (45 cm) for scale. (A) Red mudstone/claystone alternations characteristic of paralic, tidal-influenced depositional setting belonging to the Aganane Formation. (B) Lithiotid-rich floatstone to rudstone facies deposited in the vicinity of a lithiotid bioherm. (C) Oncoid-rich rudstones deposited in a brackish and restricted lagoonal setting belonging to the Aganane Formation. Large oncoids are indicated with (on). (D) and (E) Peloid-rich grainstone bearing numerous benthic foraminifera (f) and Cayeuxia sp. (Ca) algae typical of the Aganane Formation. The cemented portions of the thin section are interpreted as birdseye structures (be). (F) Grainstone of the Tafraout Formation (AU5) with diverse allochems such as ooids (o), gastropods (g), brachiopods (br), and intraclasts (in). (G) Bioclast-rich floatstone with a mixture of coral (co), crinoid (cr), and gastropod (g) fragments; Tafraout Formation (AU5). (H) Dolomitized grainstone to packstone including ooid and bioclast allochems from the top of the Azilal Formation; ooid (o) and mollusk? bioclast (b) phantoms are highlighted. (For interpretation of the references to colour in this figure legend, the reader is referred to the web version of this article.)

shallow-marine settings within the T-OAE stratigraphic interval in the central High Atlas (Krencker et al., 2015). Interval 2 is also positioned a few meters above the last lithiotid bed; lithiotids are believed to go extinct at the T-OAE (Krencker et al., 2015; Brame et al., 2019).

5.2. Ouguerd Zegzaoune

5.2.1. Stratigraphy

The Ouguerd Zegzaoune section (Fig. 3) is approximately 275 m thick and is located in the Dades Valley, 5 km east from the village of Ait Marghad (Table 1). The lower 240 m of the section was previously described and reported by Krencker et al. (2015, 2019) but the upper 35 m of the section are new observations (Tafraout Formation). The first 20 m of the total section correspond to the uppermost part of the clastic-dominated Tagoudite Formation and consist of fissile claystone intervals interbedded with siltstone beds. Up section, this fissile interval grades progressively into medium-grained sandstones capped by ooid-rich grainstones marking the bottom part of the Tafraout Formation. The stratigraphic interval between 20 m and 85 m includes three coarsening upward sequences with decreasing thicknesses of 30 m, 20 m, and 10 m from the bottom to the top, respectively.

These coarsening upward sequences have a fissile marlstone or claystone interval at their base and grade upward into ooid-rich grainstones with common herringbone cross-stratification. The last coarsening upward sequence is capped by a 40-m-thick tempestite-dominated interval including: i) red fissile claystones interfingering with wavy-laminated siltstones; ii) siltstones to fine-grained sandstones with non-amalgamated hummocky cross stratification; and iii) siltstones to fine-grained sandstones with amalgamated hummocky cross stratification. From 130 m to 150 m, storm deposits are replaced by massive ooid-rich grainstones (Krencker et al., 2015). From 150 to 240 m, the stratigraphy consists of limestone to marlstone alternations including bioclastic wackestone to packstone beds laterally grading into floatstone to rudstone beds and coral framestones (e.g. 189–198 m and 227–231 m); to date, these coral bioherms are the oldest post-T-OAE coral reefs discovered. Rare ooid-rich grainstones are also documented within this interval. Allochems consist of abundant brachiopods, corals, diverse mollusks, and crinoid ossicles. The next 17 m of the section is dominated by multiple coarsening upward sequences; the base of these sequences are marlstone intervals, including erosive thin carbonate beds, which are replaced up-section by 1–2-m-thick packstone beds with common hummocky cross stratified bedding and wave ripples on bed tops. From 257 to 263 m, the coarsening upward sequences are still observed but the hummocky cross stratification is absent. The last 13 m of the section corresponds to a massive stack of 10 cm thick grain-supported carbonate beds. From 263 m to 267 m, the beds correspond to recessive packstones progressively grading upward into cross-bedded ooid-rich grainstones including diverse bioclasts (e.g., crinoid and bivalve fragments).

5.2.2. Chronostratigraphic framework

55 samples were collected at the Ouguerd Zegzaoune section between 7 m and 226 m to analyze their total organic carbon isotope composition (Fig. 3). The carbon isotope profile of the Ouguerd Zegzaoune section can be divided into three intervals. Interval 1 (7–87 m) records an overall trend of increasing isotopic values from −26.5‰ to −21.5‰ modulated by $\delta^{13}C_{org}$ ratios oscillations of +/− 1‰. Interval 2 (87–150 m) is characterized by a 6‰ negative carbon isotope excursion. Interval 3 (150–226 m) records a decrease of $\delta^{13}C_{org}$ ratios from approximately −22‰ to −24.7‰ modulated by $\delta^{13}C_{org}$ ratios oscillations of +/− 1‰. At the top of Interval 2 (150 m), the brachiopods *Soaresirhynchia bouchardi* and *Pseudogibbirhynchia jurensis* have been collected (Krencker et al., 2019). These brachiopods are only found together in association in the western Tethyan realm within the Levisoni Zone (Alméras, 2000; Joral et al., 2011; Comas Rengifo et al., 2013). Hence, the brachiopod biostratigraphy strongly suggests that the negative carbon isotope excursion recorded within Interval 2 corresponds to the one associated with the T-OAE (Hesselbo et al., 2007; Krencker et al., 2015, 2019).

5.3. Taguendouft

5.3.1. Stratigraphy

The Taguendouft section (Fig. 3) is approximately 265 m thick and is located in the NW part of the central High Atlas, approximately 30 km SE of Beni Mellal (Table 1). This sedimentary succession was first described in Souhel (1996). The first 20 m of the section corresponds to limestone/marlstone alternations belonging to the Ouchbis Formation. Ammonite molds, belemnites, and oysters, as well as Zoophycos and Chondrites ichnogenera are commonly observed within this interval (Fig. 5A). The following 8 m shows an increase of the siliciclastic fraction, with the common occurrence of argillaceous marlstones, siltstones, and fine-grained sandstone beds, all enriched in wood debris.

The last carbonate bed of the Ouchbis Formation is observed at 23 m and is 70 cm thick; it contains numerous oysters, wood debris, and trace fossils (e.g., Zoophycos) and is capped by a ferruginous crust (see also Souhel et al., 1998). The Ouchbis Formation is overlain by approximately 60 m of green argillaceous marlstone and siltstone intervals rich in wood debris belonging to the Tagoudite Formation. At 66 m, there is a 30–40-cm-thick packstone bed containing wood debris, oncoids, diverse bioclasts, crinoid ossicles, and rare solitary corals fragments (see also Bodin et al., 2011). The following 25 m interval is characterized by an increasing occurrence of calcareous siltstone and fine-grained sandstone beds. This interval is overlain by a 10-m-thick coarsening upward sequence with common crossbedding; the sequence grades from argillaceous marlstones to medium-grained sandstones from the base to the top of the sequence, respectively.

Overlying this 10-m thick coarsening upward sequence is a 30-m-thick mixed siliciclastic/carbonate interval belonging to the Tafraout Formation. The first carbonate facies is observed at approximately 100 m and corresponds to a 1-m-thick rudstone rich in lithiotid valves and ooids; the contact with the underlying sandstone is sharp and erosive. The last carbonate bed of the mixed siliciclastic/carbonate interval is observed at 128 m and corresponds to a dolomitic bed including large dissolved lithiotid valves. The fine-grained lithologies include carbonate-rich claystones and clay-rich marlstones, and commonly include wood debris. Medium-grained sandstones and ooid-rich grainstones are the most common siliciclastic and carbonate textures, respectively. Crossbeds and hummocky cross stratification are common in medium-grained sandstones, and karstified surfaces are common in carbonate lithologies. Further up-section, the Tafraout Formation consists of two coarsening upward sequences. In the first sequence,

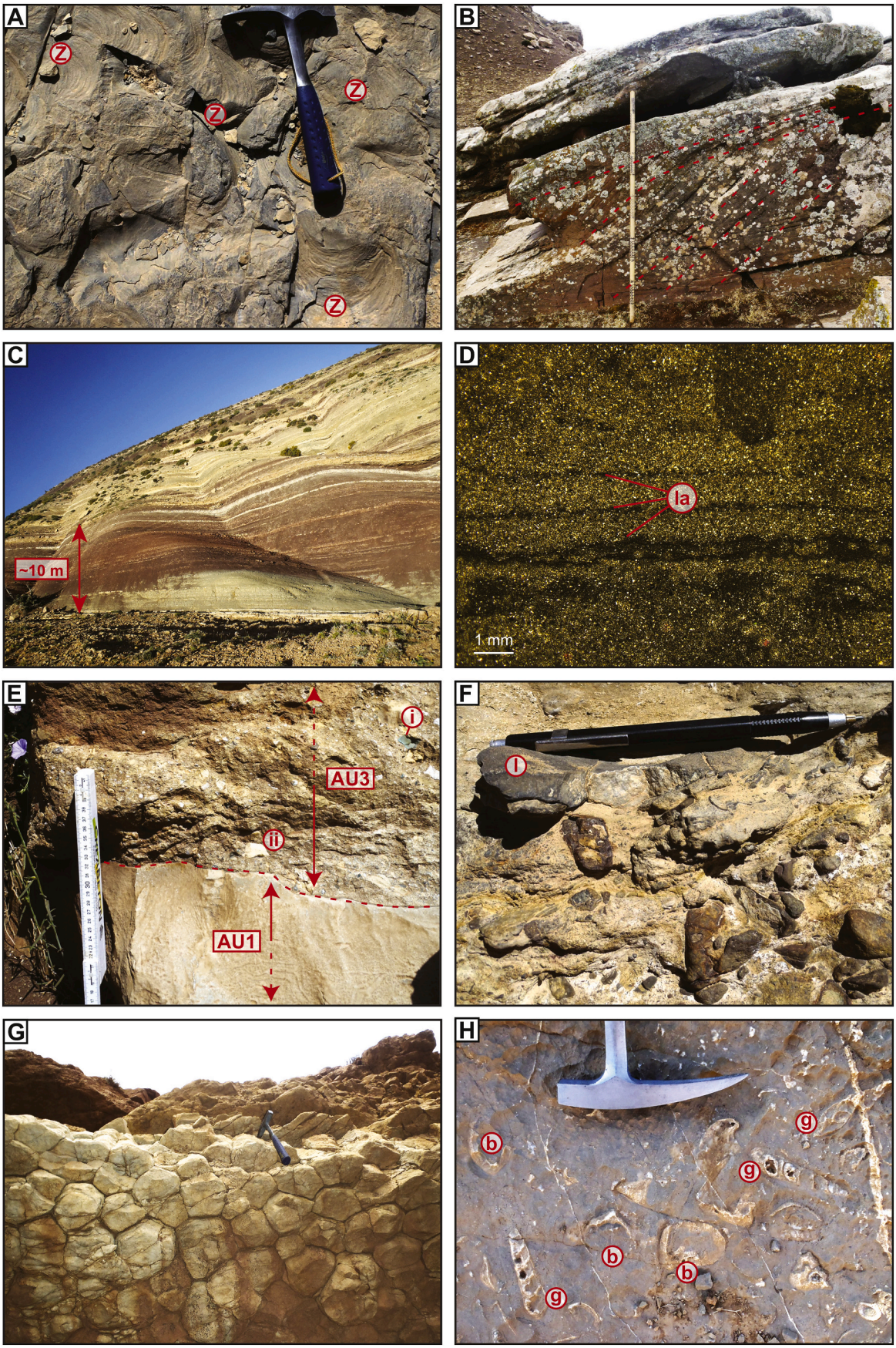

(caption on next page)

Fig. 5. Outcrop photographs and photomicrographs of upper Pliensbachian–middle Toarcian microfacies from Morocco; pencil (10 cm) and rock hammer (45 cm) for scale unless otherwise noted. (A) Numerous well-preserved (Z) Zoophycos trace fossils within the Ouchbis Formation, Dades Valey. (B) Coarse to medium sandstone with large-scale crossbeds (red dashed lines) belonging to the Tafraout Formation at the Taguendouft section (Jacob's Staff is approximately 110 cm). (C) Thick paralic reddish claystone cut by sporadic dolostone beds from the Azilal Formation at the Taguendouft section. (D) Dolo-mudstone characteristic of the Azilal Formation; (la) finely-laminated claystone layers interpreted as microbial mats. (E) Close-up on the Pliensbachian (AU1)–Toarcian (upper Polymorphum, AU3) boundary recorded in proximal settings. The boundary is erosive and covered by a polymictic conglomerates including extraclast from the (i) Paleozoic basement and (ii) reworked carbonate pebbles and cobbles from the uppermost Pliensbachian. (F) Intraformational polymictic conglomerates sitting at the very base of a lithiotid bioherm located in the Dades Valley, lithiotid shell = l. (G) Desiccation cracks in dolostone intervals; Tafraout Formation, Dades Valley. (H) Bioclast-rich floatstones to rudstones including large (g) gastropods and (b) bivalve bioclasts; this facies is typical of the Aganane Formation. (For interpretation of the references to colour in this figure legend, the reader is referred to the web version of this article.)

between 128 m and 154 m, the first 18 m of the sequence is dominated by red, fissile claystones rich in wood debris interfingering with wavy-laminated siltstones and fine-grained sandstones with common hummocky cross stratification. This interval is overlain by an 8-m-thick medium to coarse-grained amalgamated sandstone with common mega ripples and trough crossbedding (Fig. 5B). Large quartz pebbles, extraclasts, and wood debris are commonly observed within this interval. The second coarsening upward sequence occurs from 154 m to 202 m, with the first 29 m of the sequence being dominated by red claystones, calcareous claystones, and siltstones (Fig. 5C). The last 19 m of the sequence is characterized by alternations of meter-scale fissile intervals interfingering with meter-scale cross-bedded calcarenites and ooid-rich grainstones. Desiccation cracks have been observed at 181.5 m. The next 60 m of the section belong to the Azilal Formation and consist of alternations between red to greenish silt-rich claystones and dolomudstones including common birdseye textures, microbial crenulations (Fig. 5D), and desiccation cracks. The last 10 m of the section belong to the Bin el Ouidane Formation and are characterized by common ooid-rich grainstones.

5.3.2. Chronostratigraphy

96 samples were collected for total organic carbon isotope analyzes at the Taguendouft section, between 15.7 m and 244.8 m (Fig. 3). The carbon isotope profile of the Taguendouft section can be divided into four intervals. Interval 1 (18.3–113.3 m) and interval 3 (128.2–178.3 m) correspond to two negative carbon isotope excursions separated by high $\delta^{13}C_{org}$ plateau with values oscillating around −21.3‰ belonging to interval 2 (113.3–128.2 m). Interval 4 (178.3–244.8 m) corresponds to a plateau with $\delta^{13}C_{org}$ values oscillating around −22.9‰. The excursion associated with interval 1 is asymmetric and is centered around the $\delta^{13}C_{org}$ value of −26.1‰ recorded at 34.7 m and has pre- and post-excursion values of −22.7‰ and − 20.9‰, respectively. The excursion associated with interval 3 is also asymmetric and centered around the $\delta^{13}C_{org}$ value of −27.1‰ recorded at 131.8 m and has pre- and post-excursion values of −21.7‰ and − 20.8‰, respectively. In Taguendouft, the last 2.5 m of the Ouchbis Formation is dated as late Pliensbachian based on ammonites such as *Protogrammoceras celebratum, Fuciniceras cornacaldense, Emaciaticeras* sp., and *Tauromeniceras elisa* (Souhel et al., 1998). The Pliensbachian/Toarcian boundary is placed approximately where the ferruginous crust was observed at 23 m. This is based on the common occurrence of *Eodactilites* sp. and the disappearance of the late Pliensbachian ammonite fauna, which most likely indicate an earliest Toarcian age (Polymorphum Zone; Souhel, 1996; Souhel et al., 1998; Sandoval et al., 2001). The rest of the section is lacking age-diagnostic fossils but according to the sequence stratigraphic correlation of Souhel et al. (1998), the Azilal Formation in Taguendouft is best assigned to the middle Toarcian–Aalenian stratigraphic interval. In Morocco, two carbonate carbon isotope excursions are recorded within the stratigraphic interval covered by the Taguendouft section at the Pliensbachian/Toarcian boundary and within the Levisoni Zone corresponding to the Pl/To and T-OAE events (Bodin et al., 2016). We correlate the carbon isotope excursion from interval 1 to the Pl/To event based on the fact that the onset of the excursion is stratigraphically positioned at the Pliensbachian/Toarcian boundary. The excursion recorded in interval 3 is correlated to the T-OAE event based on i) its stratigraphic position above the Pliensbachian/Toarcian boundary and below the middle Toarcian–Aalenian Azilal Formation, ii) its stratigraphic position above the last lithiotid-rich bed, and iii) the common occurrence of tempestites and hummocky cross stratification sedimentary features. Altogether those characteristics are typical of the T-OAE stratigraphic interval (Trecalli et al., 2012; Krencker et al., 2015).

5.4. Tamtetoucht

5.4.1. Stratigraphy

The Tamtetoucht section (Fig. 3) is approximately 140 m thick. It is located in the upstream part of the Todhra Gorges, 2 km southwest from the village of Tamtetoucht (Table 1). The basal 3-m-thick carbonate bed of the Tamtetoucht section is uppermost Pliensbachian Aganane Formation, and from 3 to 20 m, the section contains lowermost Toarcian Azilal and Tafraout formations. The bottom part of the Tamtetoucht section is characterized by a coarsening upward sequence with 10-m-thick-greenish calcareous claystones lacking coarse clastic components, which grades upward into a massive 2-m-thick wackestone to packstone carbonate bed. Allochems include common disarticulated lithiotid valves incorporated into a greenish argillaceous matrix. This 2-m-thick lithiotid bed is abruptly replaced by a recessive reddish claystone interval interfingered with cm-scale wavy-bedded siltstone horizons. This fissile interval is sharply capped by grain-supported lithologies (from 35 to 50 m), which are predominantly ooid-rich packstones to grainstones with common quartz minerals. The dominant sedimentary features are herringbone and hummocky cross stratification bedding and bioturbation observed on top of the carbonate beds. The remaining part of the section (from 50 to 140 m) includes three coarsening upward sequences characterized by fissile argillaceous marlstones at their base, which are progressively replaced by ooid-rich packstones to grainstones.

5.4.2. Chronostratigraphic framework

29 samples were collected for total organic carbon isotope analyzes from the Tamtetoucht section, between 3 and 70 m (Fig. 3). The carbon isotope profile can be divided into two intervals. Interval 1 is characterized by overall increasing $\delta^{13}C_{org}$ ratios ranging from −25.2‰ to −22.9‰ and Interval 2 is associated with a 4‰ prominent negative carbon isotope excursion. Interval 2 is positioned directly above the last occurrence of the lithiotid-rich carbonate bed within the stratigraphic interval rich in wavy-bedded siltstones interpreted as distal storm deposits. Interval 2 is interpreted to be the T-OAE carbon isotope excursion based on its geochemical characteristics and its position in the stratigraphic column right above the last occurrence of lithiotid, which is similar to the expression of the T-OAE in the Dades Valley sections (Krencker et al., 2015; Bodin et al., 2016).

5.5. Facies description and depositional environment of the studied sections

Based on field observations, published literature, hydrodynamic regime, paleoecology of faunal content, and thin sections, 13 facies associations were determined. These facies associations characterize three depositional environments ranging from inner to outer platform setting and are detailed in Table 2.

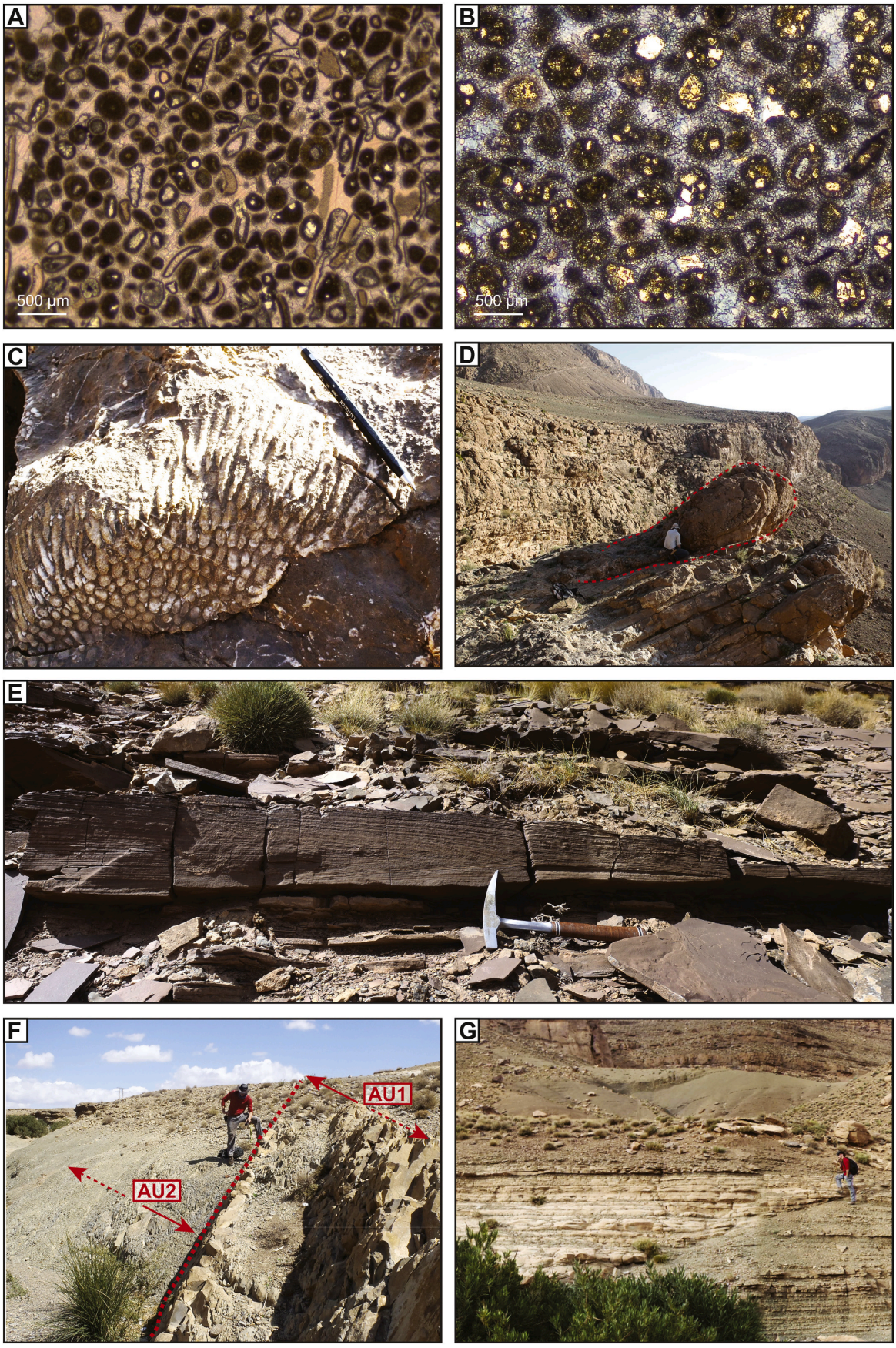

(caption on next page)

Fig. 6. Outcrop photographs and photomicrographs of lowermost to middle Toarcian lithostratigraphic formations; pencil (10 cm) and rock hammer (45 cm) for scale unless otherwise noted. (A) ooid-bioclast-rich grainstone characteristic of the Tafraout Formation. (B) Coated grains/ooid-rich grainstone found within the storm-influenced zone belonging to the T-OAE stratigraphic interval (Tafraout Formation; AU4). (C) Close-up on a phaceloid coral colony in the coral framestone, Choucht Formation. (D) Coral bioherm (red dashed line) commonly found in the Choucht Formation, Dades Valley. (E) Typical hummocky cross stratification ubiquitous in Morocco within the T-OAE storm-dominated stratigraphic interval, Dades Valley. (F) Transition between the uppermost Pliensbachian (AU1) and the lowermost Toarcian (AU2) recorded at the Foum Tillicht section. Noticed how the typical mudstone/marlstone alternations characteristic of the Ouchbis Formation (AU1) is abruptly replaced by the siliciclastic-dominated Tagoudite Formation (AU2). (G) Deep-water turbiditic channel observed at the base of the Tagoudite Formation in the Dades Valley. (For interpretation of the references to colour in this figure legend, the reader is referred to the web version of this article.)

5.5.1. Paralic and Tidal flat depositional environment

The tidal flat environment comprises four facies types. Facies 1a: Cross-bedded polymictic conglomerates composed of 5 cm sub-rounded to rounded clasts of dolo-packstones, dolo-mudstones, and packstones, as well as cm-scale angular to sub-angular extraclasts of metamorphic rocks (Fig. 5E, F). These conglomerates are most likely associated with river-dominated channels located in paralic settings. Facies 1b: Similar to facies 1a but without extraclasts of metamorphic rocks; these conglomerates are best assigned to tidal channel infill. Facies 1c: Monotonous supratidal claystones interfingering with microbialitic crenulated mats and desiccation cracks (Fig. 5G); claystone intervals are rich in continental organic matter such as wood debris and have a poor faunal content. Facies 1d is a subtidal peloid-rich grainstones with abundant algae (Fig. 4D), benthic foraminifera (Fig. 4E), and common oncoids (Fig. 4C), gasteropod and bivalve bioclasts (Fig. 5H). *Arenicolites* ichnogenera is common sedimentary features in these deposits together with birdseye texture (Fig. 4D). Facies 1e: Intertidal sandflat facies composed of ooid-rich packstones to grainstones with diverse crossbedding structures including wave ripples, flaser crossbedding, and herringbone cross-stratification (Fig. 6A, B). Other components found in this facies are bioclasts, lithoclasts (quartz, glauconite), and peloids. Facies 1 f: Medium to coarse-grained amalgamated sandstone with common mega ripples and trough crossbedding (Fig. 5B). Large quartz pebbles, extraclasts, and wood debris are commonly observed within facies 1 f.

5.5.2. Open marine depositional environment

The open marine environment is composed of six different facies types. Facies 2a: coral framestones in association with microbial bindstones, which typically form m-scale bioherms (Fig. 6C, D). Facies 2b: bivalve framestones which form biostromes and small bioherms (Fig. 4B; laterally extensive but only a few meters thick). Laterally, bioherms and biostromes belonging to facies 2a and 2b evolve into rudstones and floatstones. Other components are peloids, brachiopods, gastropods, echinoderms, and diverse bioclasts (see also Brame et al., 2019). Facies 2c: corresponds to m-scale fissile marlstone to claystone intervals incised by limestone beds. These limestone beds consist of wackestones to packstones bearing diverse biogenic fragments including echinoderms, bivalves, gastropods, cephalopods, and brachiopods. Common sedimentary features are *Thalassinoides* trace fossils in the fissile marlstone to claystone intervals. Facies 2d and 2e both correspond to storm deposits. The shallowest, facies 2d, consists of siltstones to fine-grained sandstones and occasionally medium-grained sandstones presenting amalgamated hummocky cross stratification (Fig. 6E). Toward deeper environmental settings (facies 2e), hummocky cross stratification become non-amalgamated and are separated by fissile claystone intervals interfingering with wavy-bedded siltstone beds. Lithoclasts, plant debris (i.e., wood fragments), mollusk fragments are commonly found in 2d and 2e, with rare ooids.

5.5.3. Deep platform depositional environment (outer platform)

Three facies types comprise the deep platform depositional environment. Facies 3a: Marlstone/limestone alternations; limestone beds dominated by mudstones to wackestones and sporadically by packstones (Fig. 6F). Limestone and marlstone interval thicknesses range from cm to m-scale with a marlstone/limestone ratio varying from 1:1 to 3:1. Limestone beds belonging to facies 3a exhibit a diverse ichnofacies dominated by softground ichnogenera such as *Zoophycos* (Fig. 5A), *Arenicolites*, and, occasionally, *Chondrites*. *Thalassinoides* ichnogenus is predominantly observed within fissile marlstone intervals. The macrofaunal content of facies 3a includes ammonites, belemnites, echinoderms, oysters, and gastropods; the microfaunal content is dominated by foraminifera and ostracods. Facies 3b: Claystones incised by siltstone to fine-grained sandstone turbidites (Fig. 6G). Many sedimentary features belonging to the Bouma sequence are preserved, such as groove marks and flute casts on the base of the beds, cm-scale high velocity regime planar-laminated beddings, linguoid ripples, and parallel laminations. Also common in this depositional environment are slump structures that are meters to tens of meters in scale. There are few macrofossils observed in facies 3b, but the majority are cephalopods, with rare specimens of ophiuroid impressions observed. Microfossils are more abundant and are predominantly foraminifera and ostracods. Other allochems include glauconite, quartz, and plant debris (i.e., wood fragments). Facies 3c: Fissile argillaceous facies. This facies consists of claystone intervals (several meters in thickness) interfingering with thin wavy-bedded siltstone beds. Common sedimentary features are *Thalassinoides* burrows; bioclasts, plant debris (i.e., wood fragments) are found inside the fissile intervals. Foraminifera and ostracods are the dominant fossils, with rare cephalopods.

5.6. Allostratigraphic units: description and interpretation

Based on published and newly acquired sedimentological evidence, six different allostratigraphic units (AU) are recognized within the upper Pliensbachian–uppermost Toarcian interval in the central High Atlas Basin. Each AU is characterized by a specific set of carbonate producers, siliciclastic content, and architecture. Hence, they represent distinct phase of carbonate factory development or demise. AUs 1, 3, and 5 are associated with carbonate-dominated systems, whereas AUs 2 and 4 are related to siliciclastic-rich systems. The proximal–distal facies organization along the shelf for each AU is detailed in Fig. 7.

5.6.1. AU1: the upper Pliensbachian lithiotid and coral platform

AU1 (Fig. 7A) is dominated by a photozoan ecosystem. This is exemplified by the presence in inner to middle platform settings of green algae, photosymbiotic bivalves (*Opisoma* sp.), hermatypic corals (Fig. 6C, D), and oligotrophic foraminifera (Fig. 4E; Aganane and Choucht formations). The inner to middle platform settings are also rich in diverse gastropods and bivalves such as *Cochlearites loppianus*, *Lithioperna scutata*, *Gervilleioperna* sp., and *Mytiloperna* sp. (Brame et al., 2019). The presence of echinoderms, brachiopods, and cephalopods characterizes the middle to outer platform settings (e.g., Choucht, Aberdouz, and Ouchbis formations). Carbonate ooze was shed from the inner and middle platform, which controlled the sedimentation of the outer platform (Fig. 6F); this led to the formation of the marlstone/limestone alternations of the Ouchbis Formation. Lithiotid biostromes dominated the inner platform setting behind ooidal shoals, which created restricted lagoons where marlstones, peloids, oncoids, and diverse bioclasts accumulated. The supratidal setting consisted of claystone and microbial mat alternations typical of sabkha environments (particularly during the late Pliensbachian at the Aghbalou N'Kerdous section) and red marlstones rich in carbonate nodules interpreted as calcrete.

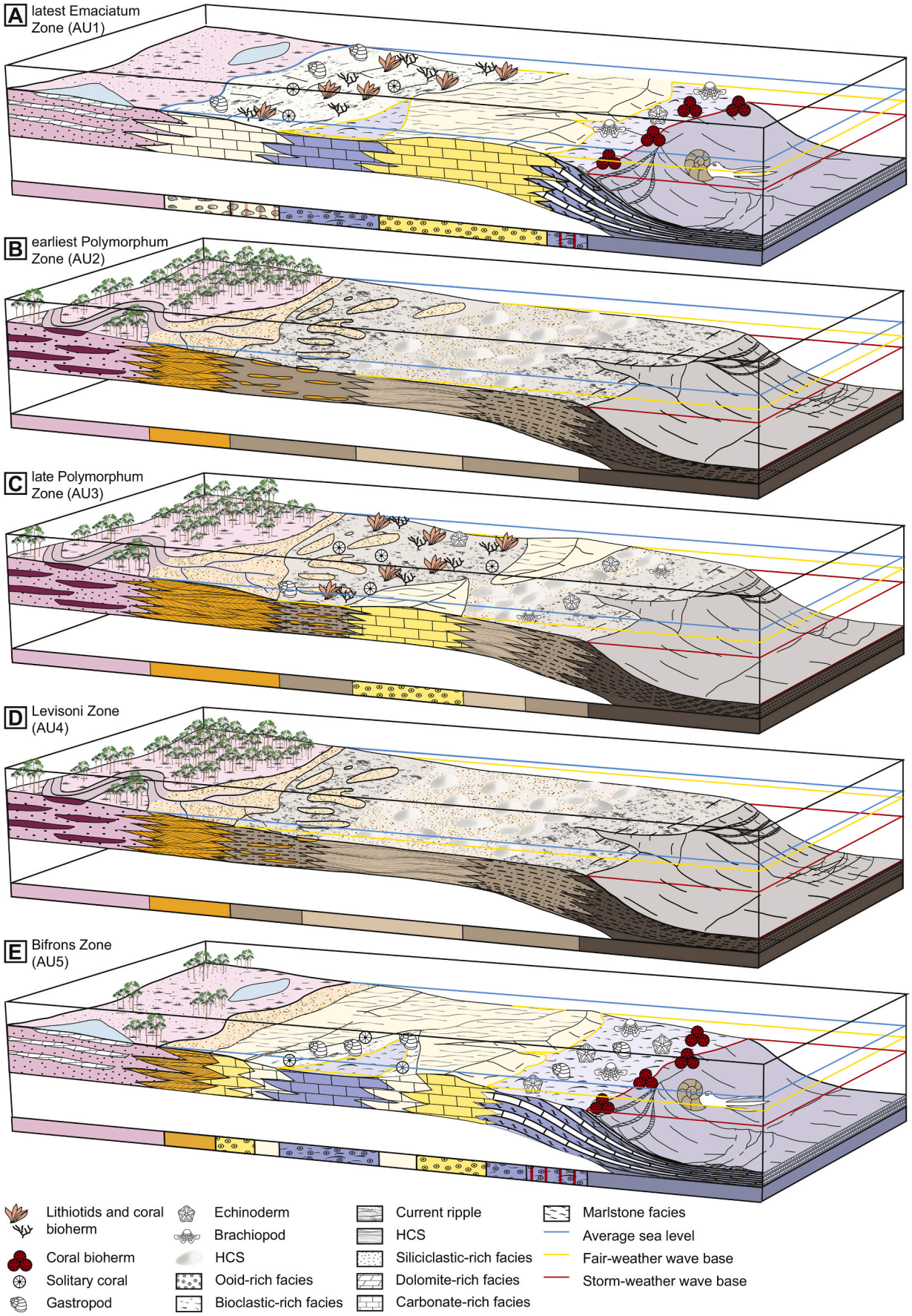

Fig. 7. Allostratigraphic unit (AU) depositional models for the late Pliensbachian–middle Toarcian. The colour coding corresponds to the facies in Table 2. See text for explanation.

Proximal settings are also characterized by the common occurrence of evaporites (gypsum). Altogether, the presence of oligotrophic organisms and compounds commonly found in tropical seas (e.g. shallow-water corals, ooids) as well as the common occurrence of calcrete and evaporites in paralic settings indicate that AU1 is best assigned to a photozoan carbonate system located within a warm semi-arid to arid climatic belt.

5.6.2. AU2: the lower Polymorphum siliciclastic-rich shelf (lowermost Toarcian)

The uppermost Pliensbachian carbonate platform (AU1) is abruptly replaced by siliciclastic deposits (AU2; Figs. 6F, 7B). In distal outer platform settings, the marlstone/limestone alternations from the Ouchbis Formation are replaced by monotonous claystones from the Agoudim Formation or, in more proximal settings, by the siliciclastic-rich (turbidites) Tagoudite Formation. The macrofossil assemblage associated with AU2 is poor and mostly represented by cephalopods and echinoderms. Field observations hence suggest a severe demise of the carbonate factory in AU2, as also indicated by a significant drop of the carbonate content from the top of the Spinatum to the lowest Polymorphum Zones in the Middle Atlas and central High Atlas basins (from 80% to 25%, and from 50% to 20%, respectively) Ait-Itto et al., 2018, and Boulila et al., 2019), with minimum values reached within the lower Polymorphum Zone. The nannofossil abundance also declines at the Pliensbachian/Toarcian boundary, and reaches a minimum just below the onset of the T-OAE carbon isotope excursion (Bodin et al., 2010). To date, there is no evidence of continental or inner platform facies allocated to the lower Polymorphum Zone in Morocco. We hypothesize that this is most likely due to the fact that those settings were areas of sediment bypass. The absence of carbonate lithologies within intervals interpreted as offshore environments most likely indicates an almost complete shutdown of the neritic carbonate factory during the earliest Polymorphum Zone (Bodin et al., 2010, 2016; Ait-Itto et al., 2018; Boulila et al., 2019). It is, however, currently impossible to be absolutely certain that neritic carbonate productivity was completely shutdown during the earliest Polymorphum Zone, but if it was still active, it would have been severely reduced and likely not preserved. Moreover, the Polymorphum Zone stratigraphy is marked by the ubiquitous occurrence of plant debris (i.e., wood fragments) and the disappearance of evaporites in proximal settings. Those characteristics strongly contrast with the uppermost Pliensbachian units, which lack wood or other plant debris and are rich in evaporites. Based on the abrupt increase of the coarse- to fine-siliciclastic content, the appearance of plant debris, and the disappearance of evaporites, AU2 is best assigned to a siliciclastic-dominated system located within a humid climatic belt.

5.6.3. AU3: the upper Polymorphum mix carbonate-siliciclastic platform (lower Toarcian)

Progressively, the siliciclastic setting of AU2 is replaced by the mixed siliciclastic-carbonate system from AU3 (Fig. 7C). In tidal settings, facies are dominated by ooid-rich grainstone beds frequently interfingering with polymictic conglomerates including fragments of metamorphic rocks (Fig. 5E, F; facies 1a). AU3 marks the reappearance of carbonate facies and especially the recovery of lithiotid-coral bioherms (Fig. 5F) located behind ooidal shoals, within the inner platform depositional setting (Brame et al., 2019). The lithiotid-rich facies is similar to the upper Pliensbachian assemblage and still includes *Cochlearites loppianus, Lithioperna scutata*, *Gervilleioperna* sp., but biostromes are dominated by *Cochlearites loppianus*. The faunal content also includes brachiopods, gastropods, bivalves (including *Opisoma* sp.), and echinoderms (Brame et al., 2019). In outer platform settings, the lithology is still dominated by monotonous fissile muddy argillaceous intervals highlighting a decrease in carbonate productivity and/or more detrital input than during the late Pliensbachian (AU1). Hence, AU3 strongly differs from the uppermost Pliensbachian carbonate-dominated AU1 due to i) the absence of evaporites-rich facies; ii) the low proportion of foraminifera- and.

oncoid-rich facies; and iii) the common occurrence of coarse-siliciclastics and wood or other plant debris. Overall, AU3 is best assigned to a mesotrophic mixed carbonate-siliciclastic system located within a warm humid climatic belt.

5.6.4. AU4: the Levisoni storm-dominated platform (lower Toarcian)

Similar to the transition from AU1 to AU2, the change from AU3 to AU4 (Fig. 7D) is abrupt and characterized by a remarkable lithological contrast. The ooid-rich grainstones allocated to the inner platform depositional setting from AU3 are abruptly replaced by fine-grained siliciclastics interfingering with wavy-bedded siltstones interpreted as distal storm-deposits (Table 2; i.e., facies 2d and 2e). In proximal depositional settings, the base of the Levisoni Zone is dominated by quartz-rich red siltstones. Nevertheless, the presence of small-size ooids included within hummocky cross stratified beds (Fig. 6B; facies 3b), and the occurrence of meter-thick ooid-rich grainstone beds (facies 1e; see also Krencker et al., 2014) within the middle part of the Levisoni Zone, might indicate that the abiotic carbonate production was not completely shut down. This uncertainty concerning the presence of carbonate facies in shallow-marine settings during the deposition of AU4 highly depends on the chemostratigraphic correlations and whether or not the carbonate facies at the very bottom of the Levisoni Zone should be included within the zone or not. In any case, the principal characteristics of AU4 are still the ubiquitous occurrence of storm-deposits, including common hummocky cross stratification structures (Fig. 6E; Krencker et al., 2015), the depauperate fauna, and notably the complete disappearance of lithiotid-rich facies, as well as the very common occurrence of plant debris (i.e., wood fragments). Toward outer platform and basinal settings, storm deposits grade into turbidites (facies 3b). AU4 is best assigned to a siliciclastic system that transitions back to a mixed or carbonate system affected by recurrent storm events. It was most likely deposited within a warm humid climatic belt, as inferred from the presence of wood debris and ooid-rich facies.

5.6.5. AU5: the early–middle Toarcian ooid-dominated platform

The middle Toarcian marks the progressive recovery of the biotic carbonate producers within an ooid-dominated carbonate factory. Field observations indicate a very efficient production and preservation of ooids (Fig. 7E) characterized by the broad lateral expansion of meter-scale ooid-rich grainstone beds including common herringbone cross-stratification (e.g. facies 1e). In outer platform settings, ooid-rich grainstone beds are replaced by wackestone to packstone beds including abundant and diverse heterotrophic faunal bioclasts, such as cephalopods, brachiopods, echinoderms, and gastropods (facies 2c). Occasionally, small-to-medium sized (50–200 cm in stratigraphic thickness) coral patch reefs have been observed in inner to middle platform settings in the Ouguerd Zegzaoune and Ait Athmane localities. The abundance of plant debris (i.e., wood fragments) decreased drastically through AU5. Together with the disappearance of coarse-siliciclastic material in this allostratigraphic unit, this might indicate the return to less humid conditions. Based on its faunal and sedimentological characteristics, AU5 is best assigned to an oolitic, mixed heterotrophic/oligotrophic platform, deposited under a warm and relatively dry climate.

6. Discussion

6.1. Regional siliciclastic influx in tune with global continental weathering changes

In Morocco two major episodes of carbonate platform shutdown occurred at the Pliensbachian/Toarcian boundary (AU 2) and at the transition between the Polymorphum and the Levisoni Zones (AU4, i.e., the onset of the T-OAE), respectively. It is highly unlikely that those

carbonate factory collapses were related to an abrupt increase in the subsidence rate as suggested for the Sinemurian and at the Sinemurian/Pliensbachian transition in the central High Atlas (Lachkar et al., 2009). Indeed, our chemostratigraphic calibration indicates that AU2 and AU4 were deposited during the Pl/To and the T-OAE events. These two carbonate platform shutdowns are hence coeval with previously documented biotic turnovers (e.g., Little and Benton, 1995; Harries and Little, 1999; Cecca and Macchioni, 2004; Mattioli and Pittet, 2004; Mattioli et al., 2008, 2009; Dera et al., 2010; Suan et al., 2010; Caruthers et al., 2013, 2014; Martindale and Aberhan, 2017) and significant perturbations to both global climate and the carbon cycle, best recorded by significant carbon isotope excursions in inorganic and organic material worldwide (Hesselbo et al., 2000; 2007; Al-Suwaidi et al., 2010; Caruthers et al., 2011; Gröcke et al., 2011; Guex et al., 2012; Hermoso et al., 2013; French et al., 2014; Ullmann et al., 2014, 2020; Bodin et al., 2016; Them et al., 2017a; Fantasia et al., 2018a; Ruebsam et al., 2019, 2020b; Ruebsam and Al-Husseini, 2020). At both events, one significant consequence of the carbon-cycle perturbation was enhanced continental weathering on a global scale, related to a warmer climate that induced a switch to more humid conditions (Weedon and Jenkyns, 2003). This is documented by strontium and osmium isotope patterns; at the Pliensbachian/Toarcian boundary the strontium isotope ratio shifts from a mantle-derived to a continental crust-derived signature (McArthur et al., 2000) and a high amplitude osmium anomaly is recorded both at the Pliensbachian/Toarcian boundary and within the T-OAE interval (Cohen et al., 2004; Percival et al., 2016; Them et al., 2017b). Hence, both strontium and osmium isotope proxies are evidence for increased precipitation and continental weathering at a global scale at the Pliensbachian/Toarcian boundary and during the T-OAE.

The sedimentological characteristics of AU2 and AU4 are in agreement with this scenario. Both AUs are characterized by: i) a drastic increase of the coarse-siliciclastic input into the basin; ii) the ubiquitous presence of plant debris (i.e., wood fragments); and iii) the absence of evaporite-rich interval and semi-arid paleosoils (e.g., calcrete), which is in stark contrast to the upper Pliensbachian strata. These sedimentary features are compelling evidence for increased humidity and riverine input in the basin during these times of major global climatic change. Furthermore, these sedimentological observations are consistent with a twofold increase of nutrient levels during the early Toarcian as inferred from phosphorus content proxy in the central High Atlas Basin (Bodin et al., 2010), in Portugal (Fantasia et al., 2019a), and in Switzerland (Montero-Serrano et al., 2015; Fantasia et al., 2018b).

6.2. Source of siliciclastic materials

The common presence of metamorphic and igneous (granitic) rock pebbles within the Toarcian siliciclastic beds in the central High Atlas Basin indicates that the siliciclastic material must be derived from Paleozoic or Proterozoic basement rocks, as those are the only suitable source material for these kinds of lithology in Morocco. This excludes de facto an intrabasinal source for these siliciclastics, given that Paleozoic and Proterozoic rocks were not exposed within the central High Atlas Basin during the Early Jurassic (Teixell et al., 2003; Frizon de Lamotte et al., 2008). Around the central High Atlas Basin, Paleozoic and Proterozoic rocks are currently exposed to the south in the Anti-Atlas, to the west in the Massif Ancien and Jebilet, and to the north in the Meseta Centrale (Fig. 8). For the Anti-Atlas and Massif Ancien, basin geometry and general stratigraphy indicate that these pre-Mesozoic basement rocks were subaerially exposed during the Jurassic (Frizon de Lamotte et al., 2008) and could thus be the source of the siliciclastic material.

Low-temperature thermochronology data (apatite fission track and [U−Th]/He analysis) can provide further constraints on the source of the siliciclastic material. Hence, thermochronology data from the western and central Anti Atlas have recorded around 40 °C cooling from Triassic to Middle Jurassic (Malusa et al., 2007; Saddiqi et al., 2009; Ruiz et al., 2011; Oukassou et al., 2013; Lepretre et al., 2018). These data can be interpreted in terms of tectonic uplift, erosion of the overburden, or a combination of both processes. A similar cooling event during the Early Jurassic is, however, limited if not absent in the eastern Anti-Atlas (Malusa et al., 2007) and in the Meseta (Ghorbal et al., 2008; Saddiqi et al., 2009); both localities show a monotonous temperature/time profile or warming during this time interval. The latter thermochronology data pattern indicates the absence of significant uplift and/or erosion of these areas. Therefore, based on the low-temperature thermochronology dataset, as well as the distribution of coarse-siliciclastic material located in the western part of the central High Atlas, we suggest that the source of coarse-siliciclastic sediments during the early Toarcian was the western and central Anti Atlas (Fig. 8). This hypothesis is further supported by the lack of coarse-siliciclastic sediment deposits in the eastern central High Atlas, which is most likely due to the absence of significant topography nearby. Alternatively, if coarse-siliciclastic sediments were deposited in the eastern central High Atlas, they must have then been subsequently winnowed into deeper environment settings following the Pliensbachian/Toarcian carbonate factory shutdown.

6.3. Carbonate factories and productivity fluctuations in the NW Tethys

With the establishment of the comprehensive dataset from Morocco, the timeline of neritic carbonate productivity in the central High Atlas Basin can be compared to previously published sedimentological and geochemical records from around the globe. These records are discussed into the context of global Pliensbachian–Toarcian paleoenvironmental disturbances.

In the NW Tethys, the Pliensbachian/Toarcian boundary corresponds to the onset of a major carbonate productivity crisis ending in the middle Toarcian (Dromart et al., 1996; Ettinger et al., 2020). This interpretation is supported by *Schizosphaerella* spp. size analyzes showing a dwarfism of different specimens, which has been linked to a biocalcification crisis (Mattioli et al., 2008), as well as an increase in opportunistic forms of benthic foraminifera coeval with an overall decrease in foraminifera diversity (see Ruebsam et al., 2020a for a review). In deeper-water settings of Morocco (Martinez et al., 2017; Ait-Itto et al., 2018; Boulila et al., 2019); Portugal (Suan et al., 2008), Spain (Danise et al., 2019), England (Kemp et al., 2011), France (Hermoso et al., 2012),) and Switzerland (Montero-Serrano et al., 2015; Fantasia et al., 2018b), the Pliensbachian/Toarcian boundary marks the onset of an abrupt and significant (> 20%) decrease of the total carbonate content, which indicates that adjacent platforms ceased or substantially reduced their carbonate production. That said, the low latitude carbonate production was not entirely halted and seems to have persisted in a few localities in Italy (Trecalli et al., 2012) and Croatia (Sabatino et al., 2013). However, this vision is not unanimous and some authors posit that the carbonate factory in these areas also collapsed (Ettinger et al., 2020). This discrepancy might come from the biostratigraphic control on these two latter localities, which is relatively poor, raising doubt on the exact status of carbonate factory across the Pliensbachian/Toarcian boundary at these localities. In Morocco, the Pliensbachian/Toarcian boundary corresponds to the most severe change concerning the carbonate productivity within the studied interval. Indeed, in deep depositional settings (> 100 m, i.e., the Tagoudite and Agoudim 1 Formations) carbonate beds are absent and the overall carbonate content is at the lowest levels (Ait-Itto et al., 2018; Boulila et al., 2019). Other noticeable changes include the disappearance of evaporites in supratidal setting (such as those reported within the uppermost Pliensbachian in Aghbalou N'Kerdous), coral extinctions (Vasseur, 2018; Brame et al., 2019), and the common occurrence of plant debris (i.e., wood fragments) in all observed lower Toarcian depositional settings. Overall, this pattern is interpreted to be indicative of a major climatic change from semi-arid to humid conditions.

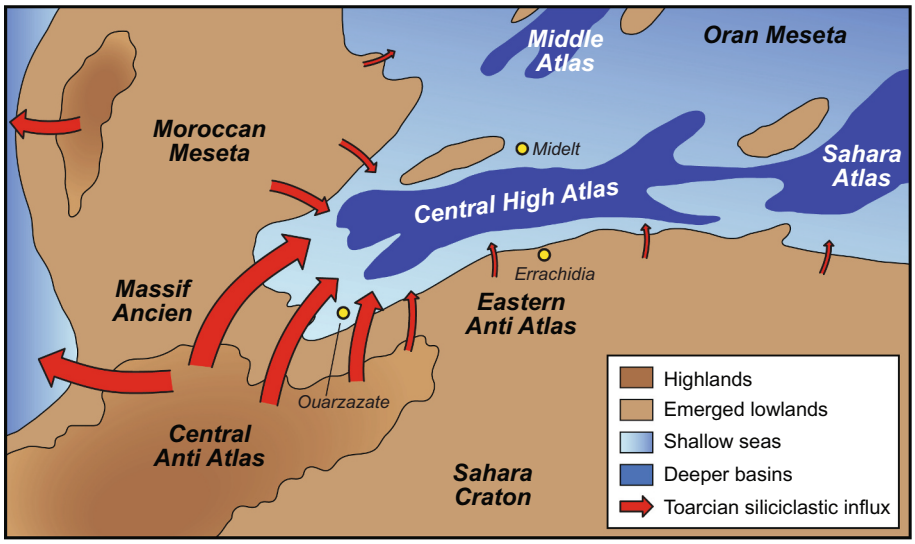

Fig. 8. Schematic depositional map for the early–middle Toarcian highlighting the broad source–sink relationship for the central High Atlas Basin (modified from Bassoulet et al., 1993, Du Dresnay, 1971, and Blomeier and Reijmer, 1999). Size of arrows represents relative volume of sediment flux.

In the aftermath of this first carbonate productivity crisis, the presence of fine-grained micritic carbonate in upper Polymorphum (lower Toarcian) hemipelagic settings from Italy, Portugal, and Spain (Mattioli and Pittet, 2004; Suan et al., 2008; Pittet et al., 2014; Danise et al., 2019) suggests renewal of neritic carbonate production prior to the onset of the T-OAE. Fine-grained micritic carbonate beds are also reported in similar hemipelagic depositional settings and stratigraphic intervals in the central High Atlas (Bodin et al., 2010, 2011, 2016; Boulila et al., 2019), Middle Atlas (Ait-Itto et al., 2018), Algeria (Ruebsam et al., 2020a), and Tunisia (Soussi and Ben Ismail, 2000). The upper Polymorphum carbonate beds could result either from the export of material from an adjacent shallow-water carbonate system or from early diagenetic processes (Suan et al., 2008; Bodin et al., 2016). An example of one such early diagenetic/authigenic processes would be microbially mediated calcite precipitation in organic-rich facies below the water-sediment interface (Raiswell, 1988; Sass et al., 1991). Nevertheless, the recognition of uppermost Polymorphum carbonate-rich inner platform facies (AU3) in Morocco argues in favor of export from the adjacent shallow-water carbonate system.

Moreover, our results indicate a major change of the main carbonate factory from a photozoan carbonate-producing system during the latest Pliensbachian to a heterozoan-dominated carbonate-producing system during the earliest Toarcian. Indeed, the green algae and the entire oligotrophic foraminifera biota described in the Pliensbachian of the High Atlas Mountains (Septfontaine, 1985) are absent from the upper Polymorphum Zone. Within this carbonate factory recovery interval, macroscopic carbonate productivity is mainly sustained by the bivalve *Cochlearites loppianus*, commonly found in association with other heterotroph organisms, such as brachiopods, gastropods, and echinoderms and in a minor extent with corals (Brame et al., 2019). Moreover, the rare occurrence of coral-microbialite bioconstructions in inner-platform setting suggests that photozoan organisms were stressed and had only a minor contribution to the carbonate production. It is worth noting that even within this recovery interval, the siliciclastic content is high, suggesting that the carbonate production took place in turbid- and nutrient-rich water (Bodin et al., 2010; Brame et al., 2019), which explains the switch to a heterozoan-dominated carbonate factory in Morocco.

In the NW Tethys, the lower Serpentinum Zone (Levisoni Zone equivalent) is characterized by a second biocalcification crisis (Suan et al., 2008; Hermoso et al., 2012; Clemence, 2014). Observations from Morocco are in line with this scenario and clearly indicate a drastic drop in neritic carbonate productivity, which is replaced by increased-siliciclastic content in the lowermost part of the T-OAE interval (concomitant with the negative $\delta^{13}C$ shift at the onset of the T-OAE). This feature is also similar to the observations of carbonate platform exposed in the Tibetan Himalaya, and originally deposited on the open SE Tethyan margin of the southern hemisphere showing a biotic demise (Han et al., 2018). Carbonate productivity, however, did not cease for the entire T-OAE interval, but recovered during the negative $\delta^{13}C$ plateau phase, switching into a chemical/microbial-dominated precipitation mode as opposed to the biogenic-dominated mode observed previously. This is well expressed in the sedimentary archive in Morocco with the ubiquitous occurrence of ooid-rich beds. The intra-T-OAE ooids are very small, less than a millimeter in diameter, and often only composed of one or a few laminae surrounding a quartz grain core (Fig. 5). Similar observations have been reported in other localities where the entire T-OAE negative CIE is also recorded in a stratigraphic interval dominated by non-fossiliferous, ooid-rich grainstone beds (Trecalli et al., 2012; Han et al., 2018; Ettinger et al., 2020).

Full carbonate factory recovery follows the T-OAE interval, with carbonate production returning to pre-T-OAE levels as inferred from the important thickness and widespread distribution of uppermost lower and middle Toarcian carbonate deposits in the central High Atlas Basin. This interval is marked by the reappearance of marine invertebrate fossils in the rock record, such as brachiopods, echinoderms, corals, and cephalopods. Coral bioherms have also been identified within the middle Toarcian at the Ouguerd Zegzaoune and Ait Athmane localities (Ettaki and Chellaï, 2005; and own observations). No lithiotids or lithiotid bioconstructions have been documented above the T-OAE interval in Morocco (Brame et al., 2019), South America (Fraser et al., 2004), Tibet (Newton et al., 2011; Han et al., 2018), or Italy (Trecalli et al., 2012). This indicates that the environmental changes associated with the T-OAE probably delivered the “coup de grâce” to the lithiotid taxa (Brame et al., 2019).

6.4. Potential cause of carbonate factory shutdown

Neritic carbonate ecosystems are sensitive to environmental and climate changes because calcite- and aragonite-precipitating organisms thrive under specific ecological conditions (Mutti and Hallock, 2003; Föllmi et al., 2006; Halfar et al., 2006; Hueter et al., 2019). In response to changing physical and/or chemical parameters (e.g. seawater temperature, oxygen, nutrient levels etc.), carbonate platforms often switch

between photozoan and heterozoan carbonate factories, or might as well change from a dominantly biotic carbonate factory (i.e., carbonate precipitated by organisms) to a chemical carbonate factory (i.e., carbonate precipitated abiotically or in the absence of biomineralizing organisms). In extreme cases, the platform may cease carbonate production entirely and drown (Schlager, 1981; Immenhauser, 2005; Bodin et al., 2006; Föllmi et al., 2006; Godet, 2013). Evidence for two major carbonate factory collapses has been recognized within the uppermost Pliensbachian–middle Toarcian stratigraphic interval in sections palinspasticaly located in the NW Tethys. Possible mechanisms that may or may not explain the cessation of carbonate production are discussed hereafter.

6.4.1. Anoxia

Low oxygen content in the water column is often a factor believed to have triggered faunal turnovers and mass extinction at the Polymorphum/Levisoni (Tenuicostatum/Serpentinum equivalent) transition (Wignall et al., 2005; Danise et al., 2019; Reolid et al., 2019; Ruebsam et al., 2020a). In the eastern part of the central High Atlas Basin, laminated black claystone horizons are also intermittently present within the T-OAE interval in the Agoudim Formation at Foum Tillicht (Martinez et al., 2017). These dark laminated claystones are interfingered with fine-grained sandstone turbidites and include common *Bositra* sp. bivalve fossils (Martinez et al., 2017). In Dotternhausen (Germany), the presence of *Bositra buchi* has been interpreted as indicative of low oxygen levels based on the enrichment of redox sensitive elements in the host sedimentary rocks (Röhl et al., 2001). It is thus possible that the deep-water setting (> 100 m) in the eastern part of the central High Atlas Basin might have suffered oxygen depletion. This assumption, however, needs to be further tested with redox-sensitive trace elements concentrations (Riquier et al., 2006; Tribovillard et al., 2006; Bodin et al., 2007; Fantasia et al., 2018a, 2018b; Montero-Serrano et al., 2015).

In contrast, deep-water settings located in the western part of the central High Atlas i) lack laminated organic-rich horizons; ii) are characterized by low total organic carbon (TOC) content (e.g. Amellago; $TOC_{average}$ < 0.5%, max TOC: 3.2%; Talghemt; $TOC_{average}$ < 0.5%, max TOC: 0.8%; Bodin et al., 2010, 2011); and iii) are lacking uranium enrichment, which altogether indicate that the sediment-water interface and overlying water column was most likely not anoxic (Bodin et al., 2011). Similar observations within the T-OAE stratigraphic interval have been made in deep-water settings in Portugal (Hesselbo et al., 2007; Fantasia et al., 2019a) and Switzerland (Fantasia et al., 2019b).

In regions where shallow-marine environments have been preserved such as in Italy (Trecalli et al., 2012), Slovenia and Montenegro (Črne and GoriČan, 2008), Croatia (Sabatino et al., 2013), Portugal (Pittet et al., 2014), and Morocco (this study), characteristic laminated organic-rich facies are lacking within the T-OAE stratigraphic interval. In Croatia, the high bioturbation density characterizing the “spotted limestones” indicates that the water column was well oxygenated (Sabatino et al., 2013). In Morocco, the T-OAE stratigraphic interval is characterized by reddish oxidized claystones with clear evidence of storm activity (Krencker et al., 2015), which almost certainly implies a well-oxygenized water column during the T-OAE. Dark laminated claystones are present prior to the T-OAE interval within the lithiotid-coral framestones in the Dades Valley, but those are interpreted as possible short-lived events, such as seasonal episodes of oxygen depletion (possibly associated with phytoplankton blooms), or depleted oxygen within lagoonal sediments. The fact that organisms recovered directly above the black laminated horizons seems to indicate those episodes were very local and only had a minor effect of the benthic community.

Overall, the lack of evidence for anoxic conditions in Morocco indicates that the expansion of the minimum oxygen zone during the T-OAE never reached the continental shelf at the studied localities. Therefore, it is unlikely that anoxia was the primary mechanisms responsible for the neritic carbonate crisis reported in the northern Gondwana margin sections during the Pliensbachian and Toarcian. Based on the sedimentological and geochemical dataset to date (Danise et al., 2019; Ruebsam et al., 2020a), it appears that anoxia was probably a killing mechanism solely during the T-OAE and mostly in deep-water settings in the NW Tethys. Nevertheless, episodic shallow-water anoxia may have occurred in neritic settings during hyperthermal conditions associated with the T-OAE (Leonide et al., 2012; see also Hueter et al., 2019, for a discussion about platform-top seawater oxygen depletion during Oceanic Anoxic Event 1a), contributing to the weakening of the carbonate factory.

6.4.2. Ocean acidification

Several biotic trends have been used as potential evidence for ocean acidification during the Early Jurassic. Since the Early Jurassic is one of the most significant reef collapses of the Phanerozoic and was particularly selective against organisms that were likely sensitive to acidification (i.e., taxa that are physiologically unbuffered or that invest substantially in producing carbonate skeletons), Kiessling and Simpson (2011) suggested that there was strong evidence for ocean acidification as a cause of the reef collapse, albeit in concert with ocean warming. That said, in a larger database analysis, calcification was not shown to be a significant predictor of extinction during the early Toarcian (Dunhill et al., 2018). Although informative, these database studies (i.e., Kiessling and Simpson, 2011; Dunhill et al., 2018) lack the resolution to distinguish between the Pliensbachian/Toarcian stage boundary and the T-OAE; thus, these results must be regarded with caution as it may not be clear precisely when the biotic collapse occurred.

Acidification of surface marine waters has also been invoked to explain the dramatic decrease in pelagic carbonate production by nannoplankton, reduction in size of some species and maximum fragmentation of calcispheres across the T-OAE (Erba, 2004; Mattioli and Pittet, 2004; Suan et al., 2008; Hermoso et al., 2012). Recently, this concept has been challenged by the relationship between a generalized seawater temperature curve and the size of *Schizosphaerella* spp. for the Pliensbachian (Peti and Thibault, 2017). The Peti and Thibault (2017) study shows that small-size and large-size specimens are associated with warm and cold episodes, respectively. Acidification was invoked as the main killing mechanism of the lithiotids/*Palaeodasycladus* carbonate factory in Italy at the onset of the T-OAE carbon isotope excursion (Trecalli et al., 2012). The authors speculated that lithiotids and *Palaeodasycladus* calcified similarly to present-day edible mussels and *Halimeda* algae, respectively, and thus both organisms may have been similarly sensitive to increasing pCO_2.

In Morocco, the last Lower Jurassic lithiotid bed is found right below the onset of the T-OAE carbon isotope excursion, similar to the sections in Italy (Trecalli et al., 2012), Croatia (Sabatino et al., 2013) and Tibet (Han et al., 2018). In that sense, the Moroccan record supports the concept that lithiotids went extinct during the T-OAE; however, it is still unclear whether this extinction was due to a decrease of seawater calcium carbonate saturation or another process. Notably, the ooids found within the descending part of the T-OAE carbon isotope excursion (Fig. 5F) are of small-size and are characterized by very thin cortex, contrasting with ooids from surrounding stratigraphic intervals, which are much larger and have thick, multilayered laminations in the cortex. This could be interpreted as a sign of decreasing pH or carbonate saturation state (Ω) and thus ocean acidification at the onset of the T-OAE. Indeed, parameters decreasing ooid-size include high nuclei supply, low cortex growth, and a short suspension time in the water-column, which are connected to low carbonate saturation states and a low hydrodynamic regime (Sumner and Grotzinger, 1993; Trower et al., 2017; Diaz and Eberli, 2019). In Morocco, hydrodynamic conditions have been interpreted to have increased based on the common occurrence of ubiquitous record of storm deposits showing hummocky cross

stratification (Krencker et al., 2015). Therefore, in Morocco the small-size ooids observed within the T-OAE might be a consequence of low carbonate saturation and/or high nuclei supply, which can be linked to both acidification and/or enhanced sediment supply. We must caution that this interpretation is still speculative and would require more thorough grain-size and statistical analyzes to be confirmed or refuted.

Overall, the ocean acidification hypothesis is in line with the rapid and significant pCO_2 increase recorded across the onset of the T-OAE, as derived from a stomatal index study (McElwain et al., 2005) and compound-specific carbon isotope data of land plant (Hermoso et al., 2012; Ruebsam et al., 2020b). Therefore, ocean acidification could explain the carbonate factory shutdown occurring at the Polymorphum/Levisoni transition but this hypothesis still requires more compelling evidence and further investigation. Acidification events are notoriously difficult to identify in the rock record as one of their characteristics is that they destroy the record of the event, either by halting carbonate production or by dissolving the record of an event (see Greene et al., 2012). Moreover, it is important to note that no sedimentological or geochemical evidence for ocean acidification has so far been found for the Pl/To event. The significant extinction of physiologically unbuffered taxa and the reef collapse across the Pliensbachian/Toarcian boundary (Kiessling and Simpson, 2011) may provide support for acidification at the stage boundary. However, due to the poor high-precision calibration of the dataset upon which this observation is made, it is unclear whether this turnover is at the Pl/To boundary or the T-OAE event, or is a biased interpretation due to the amalgamation of both events in the "Reef Database". Hence, we speculate that ocean acidification has not taken a leading role for the major carbonate factory shutdown observed at the stage boundary, contrary to the one associated with the T-OAE.

6.4.3. Seawater temperature fluctuations

Temperature is one of the most important parameters controlling the productivity of carbonate platforms (Schlager, 2003; Halfar et al., 2006; Michel et al., 2019). During the Pliensbachian–Toarcian, global temperatures have repeatedly fluctuated from icehouse to hothouse regimes, such as during the Pl/To and T-OAE (Bailey et al., 2003; Rosales et al., 2004; Suan et al., 2010; Krencker et al., 2014; Korte et al., 2015; Baghli et al., 2020; Piazza et al., 2020; Ullmann et al., 2020). Those assumptions are based on average increase/decrease of the oxygen-isotope ratio from biocalcifiers in the NW Tethys and interpreted as reflecting warming/cooling of sea-surface temperature in this region (Dera et al., 2011a; Korte et al., 2015; Ruebsam et al., 2019; Piazza et al., 2020). Even though the oxygen-isotope values are probably influenced by salinity changes (Suan et al., 2008), indirect and independent paleotemperature proxies support the interpretation that these oxygen isotope datasets are primarily a paleotemperature indicator. Those independent proxies include the migration pattern of cephalopod species (Suan et al., 2008; Dera et al., 2011a), pCO_2 values inferred from stomatal indices (McElwain et al., 2005) and differences in the magnitude of the carbon isotope excursion recorded in land plants and marine substrates (Ruebsam et al., 2020b), and the presence of cold-climate indicators such as glendonites (Suan et al., 2011; Barth et al., 2018) and high-amplitude sea-level fluctuations (Krencker et al., 2019). Thus, the concomitance of carbonate factory shutdown and hothouse regimes might indicate a cause and effect relationship.

Conversely, numerical climate modelling indicates that within the NW Tethys epicontinental sea, sea-surface temperatures for a given latitude were most likely homogeneous (Donnadieu et al., 2011; Baroni et al., 2018). As a consequence, these temperature data cannot explain all of the sedimentological patterns. Hence, the Croatian carbonate platforms carried on producing carbonates during the T-OAE, whereas the Portuguese carbonate platform, which was located at the same paleolatitude, did not (Sabatino et al., 2013). Furthermore, a decline in the presence and abundance of larger-sized bivalve species seems to be correlated to the increase of seawater temperatures in Spain; however this relationship is not statistically supported for brachiopods (Piazza et al., 2020). Also, cephalopods were affected by the Pliensbachian/Toarcian extinction at the genera and species level, but this was independent of their affinity for cold or warm water (Dera et al., 2011a). Altogether, these observations indicate that temperature changes might not have been a proximate cause for the shutdown of carbonate production and/or faunal turnovers recorded within the studied time interval. Nevertheless, global temperature changes were likely a significant factor in the early Toarcian perturbations, triggering a cascade of environmental changes leading to the Pl/To and T-OAE events.

6.4.4. Enhanced continental weathering

Enhanced continental weathering during the Pl/To and T-OAE events led to higher siliciclastic sediment supply and increased dissolved material (organics and ions) to the oceans (Cohen et al., 2004; Dera et al., 2009b; Hermoso and Pellenard, 2014; Percival et al., 2015; Them et al., 2017b; Deconinck et al., 2020). This has the potential to alter nutrient levels, the turbidity, and salinity of the water column and as such can trigger the cessation of healthy carbonate platforms (Hallock and Schlager, 1986; Föllmi et al., 2006; Halfar et al., 2006; Godet et al., 2013). In Morocco, it has been suggested that changes in trophic levels in the NW Tethys could explain the collapse of carbonate productivity associated with the early Toarcian (Bodin et al., 2010) and environmental disturbances at the middle–late Toarcian transition (Krencker et al., 2014). This postulation is based on the increase of the total phosphorus content measured on bulk micrite samples from hemipelagic sections in Morocco (Bodin et al., 2010; Krencker et al., 2014). In Switzerland, similar results have been obtained by measuring phosphorus contents along a proximal–distal transect (Fantasia et al., 2019b). Higher trophic levels in the NW Tethys during the early Toarcian are further corroborated by nannofossil assemblages in sections located in Portugal, France, and Germany (Mattioli and Pittet, 2004; Mattioli et al., 2008; Clemence, 2014). Indeed, the Pliensbachian/Toarcian boundary event is characterized by the switch from oligotrophic to *meso*trophic nannofossil taxa such as *Similiscutum novum*, *Similiscutum finchii*, *Mitrolithus jansae*, and *Bussonius* spp. In our present study, the characterization of the main carbonate producers below and above the Pliensbachian/Toarcian crisis indicates similar results. Interestingly, places isolated from continental riverine inputs (e.g. Italy, Slovenia, Croatia, and Montenegro) seem to have maintained their carbonate production during most of the T-OAE, beside the potential effect of ocean acidification at the onset of the event (Trecalli et al., 2012; Sabatino et al., 2013; Ettinger et al., 2020). That said, it is still unclear whether or not an enhanced continental weathering was responsible for the carbonate factory shutdowns recorded in higher latitudes (Wignall et al., 2005; Leonide et al., 2012) at the Pl/To and the T-OAE intervals. In Morocco, though, it seems that enhanced continental weathering can explain the majority of the sedimentological observations for both the Pl/To and T-OAE stratigraphic intervals. Moreover, a shift to more nutrient-rich, turbid waters could account for the transition from settings conducive to photozoan carbonate producers, including coral reefs, to more heterozoan communities. Enhanced continental weathering can thus be considered a major controlling mechanism on the High Atlas carbonate factory during the Toarcian and could explain the extinctions of taxa which typically prefer oligotrophic conditions.

6.4.5. Storm activity

Tropical storms and hurricanes have the potential to stress calcifying marine organisms by changing key physical parameters in the water column and platform/shelf morphology (Ball et al., 1967; Paerl et al., 2001; Quiquerez et al., 2004; Mallin and Corbett, 2006). For instance, strong winds associated with extensive precipitation affect temperature, salinity, and nutrient inputs into shallow-marine environments. Rapid and repeated fluctuations of those parameters could deeply harm a healthy carbonate system if sustained for too long.

Interestingly, it has been observed that the T-OAE sedimentary record in the Tethys is shaped by an intensification of tropical storm events (Krencker et al., 2015; Han et al., 2018). This interpretation is based on sedimentological evidence obtained in a number of West European, Moroccan and Tibetan sections all of which cover the inner to outer neritic settings over a time interval of approximately 9 Myr.

6.4.6. Sea-level changes

Sea-level changes have often been invoked to explain extinction and origination of species. For cephalopods, it has been suggested that transgression cycles were associated with species and genera origination whereas regression cycles were associated with extinction (Sandoval et al., 2001). Interestingly, the two carbonate factory collapses during the Toarcian documented in the NW Tethys and in Morocco are all directly preceded by a major sea-level fall (Pittet et al., 2014; Krencker et al., 2019). It is hence possible that the sea-level drop related to the transient waxing and waning of polar continental ice sheet (Krencker et al., 2019), which occurred before each event, may have contributed to weaken the benthic carbonate factory by reducing the main carbonate producers' habitat space on the continental shelf. If these sea-level falls depleted the diversity or abundance of an ecological community, they may not have radiated during the subsequent deglaciation and sea-level rise, especially if the transgression was accompanied by other environmental stressors. Similar involvement of combined rapid sea-level fluctuation and environmental deterioration are also observed for other major carbonate factory demise events (e.g. Godet, 2013). This would also explain why these two events mostly affected neritic organisms more than continental or pelagic ones (Hallam, 1997; Wignall et al., 2005; Dera et al., 2011b).

6.5. Triggering mechanisms of the neritic environmental changes in Morocco

In the previous section, we provided a list of hypotheses to explain the carbonate productivity changes that coincide with carbon cycle disturbances in the NW Tethys. The listed hypotheses are non-exhaustive and most likely acted with variable intensity in each basin, or in combination. Clearly, for the relatively small area represented by the NW Tethys epicontinental sea, numerous causes can explain local, but significant, differences in the sedimentological record within the uppermost Pliensbachian–middle Toarcian. Ultimately, carbon cycle disturbances that are global can still have strong local variability. These local conditions should be considered independently in each sedimentary basin before drawing global paleoenvironmental conclusions. With this in mind, we propose hereafter to inscribe the neritic changes observed in the central High Atlas Basin within the current understanding of environmental changes and their triggers during the latest Pliensbachian–early Toarcian.

Our study suggests that the multiple changes in neritic carbonate factories are tightly tuned to environmental perturbations that were most likely paced by the pulsed activity of the Karoo-Ferrar-Chon Aike large igneous province (Fig. 9; Jourdan et al., 2008; Svensen et al., 2018). The occurrence of mercury (Hg) anomalies recorded at the Pliensbachian/Toarcian boundary, which persist after TOC normalization, have been interpreted as a fingerprint of Karoo-Ferrar-Chon Aike volcanic activity (Percival et al., 2015, 2016; Fantasia et al., 2018, 2019). Nevertheless, the mercury cycle is complex and can potentially be affected by local processes such as enhanced continental weathering (Grasby et al., 2019 for a review; Them et al., 2019). To date, it is not clear whether enhanced mercury input in the atmosphere or local weathering conditions led to mercury anomalies recorded in Toarcian strata (Grasby et al., 2019). Yet, the potential effects of the Karoo-Ferrar-Chon Aike volcanic activity likely induced multiple, synergistic effects that triggered various deleterious mechanisms (discussed above).

Hence, the initial basaltic pulses of the Karoo–Ferrar Chon Aike most likely released high concentrations of CO_2 in the atmosphere, initiating global warming events at the Pliensbachian/Toarcian, followed by a second wave of CO_2 release at the Polymorphum/Levisoni transitions (e.g. McElwain et al., 2005; Suan et al., 2010; Percival et al., 2016; Storm et al., 2020; Ruebsam et al., 2020b). During both events, high temperatures could have destabilized gas hydrates located in the permafrost areas and stored during previous cooler intervals (Ikeda et al., 2018; Krencker et al., 2019; Ruebsam et al., 2019, 2020b), reinforcing the greenhouse effect. Additionally, other factors such as thermogenic methane release from Paleozoic coal in the Karoo–Ferrar-Chon Aike province (McElwain et al., 2005; Svensen et al., 2007; but see also Gröcke et al., 2009), or oxidation of organic matter and increased terrestrial cycling (e.g. wetlands, lakes, and soils; Them et al., 2017a) could have played an amplifying role during the Pliensbachian/Toarcian and T-OAE carbon cycle perturbations.

High atmospheric pCO_2 is key factor for triggering enhanced continental weathering and runoff (e.g., Weissert, 2000; Jenkyns, 2010; Cohen et al., 2004; Bodin et al., 2010; Percival et al., 2016; Them et al., 2017b; Fantasia et al., 2018b). Based on phosphorus concentration evidence (Bodin et al., 2010; Fantasia et al., 2019b), enhanced continental weathering increased nutrient delivery to the ocean, especially in areas close to continental landmasses such as the High Atlas Basin. Given the low latitudinal setting of the High Atlas Basin, it is likely that the change from a dry to a humid climate at the Pliensbachian/Toarcian boundary proceeds from a northward expansion of the tropical humid belt. A recent study from Northern Spain suggests also that the early Toarcian warming was also accompanied by a southward expansion of the temperate humid belt (Deconinck et al., 2020), implying a narrowing of the semi-arid climatic belt in the northern hemisphere during the early Toarcian. Alternatively, it could also be suggested that the equatorial humid belt extended all the way up to Northern Spain during the early Toarcian, pushing the semi-arid climatic belt to higher latitude. The latter scenario might find support in the climatic reconstruction based on clay mineral distribution and modelling (Dera et al., 2009b; Dera and Donnadieu, 2012).

In any case, nutrification promoted deleterious shifts in neritic ecosystems, and ultimately led to carbonate platform drowning, as often observed for other carbonate factory demise events (e.g. Drzewiecki and Simo, 1997; Mutti et al., 1997; Bodin et al., 2006, 2017; Brandano et al., 2009; Föllmi et al., 2006; Föllmi et al., 2012; Godet, 2013). This mechanism is likely to have played a major role at the Pliensbachian/Toarcian boundary, as it accounts for the major change from oligophotic to meso/eutrophic conditions in the central High Atlas Basin; and hence, the disappearance of the Pliensbachian, photozoan-dominated carbonate factory (Fig. 9). It is, however, unlikely to be the sole mechanism responsible for this initial carbonate factory demise given that a heterozoan-dominated carbonate platform establishes itself in the second half of the Polymorphum Zone, a time interval when nutrient levels were still elevated in Morocco (Bodin et al., 2010). Hence, rapid sea-level rise following the late Pliensbachian sea-level lowstand, and/or “poisoning” due to the overwhelming influx of coarse siliciclastic material, could be invoked as complementary triggering mechanisms in this case.

Furthermore, the injection of CO_2 into the atmosphere can generate ocean acidification if the CO_2 injection is sufficiently rapid and massive (Hönisch et al., 2012). Such conditions are inferred for the onset of the T-OAE (e.g. Trecalli et al., 2012; Ettinger et al., 2020), but are, currently, more difficult to infer for the boundary event. Ocean acidification could have thus played a major role for the neritic carbonate factory demise occurring at the onset of the T-OAE, as supported by the presence of small-size ooids characterized by very thin cortex in this part of the stratigraphic record in Morocco. Moreover, the intensification of hurricane at that time would have certainly contributed to further weaken the sustainability of the carbonate platform, and hence contributed to this second demise event.

Recovery of neritic carbonate productivity occurred shortly after the onset of the T-OAE, at a time of persistently elevated temperatures (e.g.,

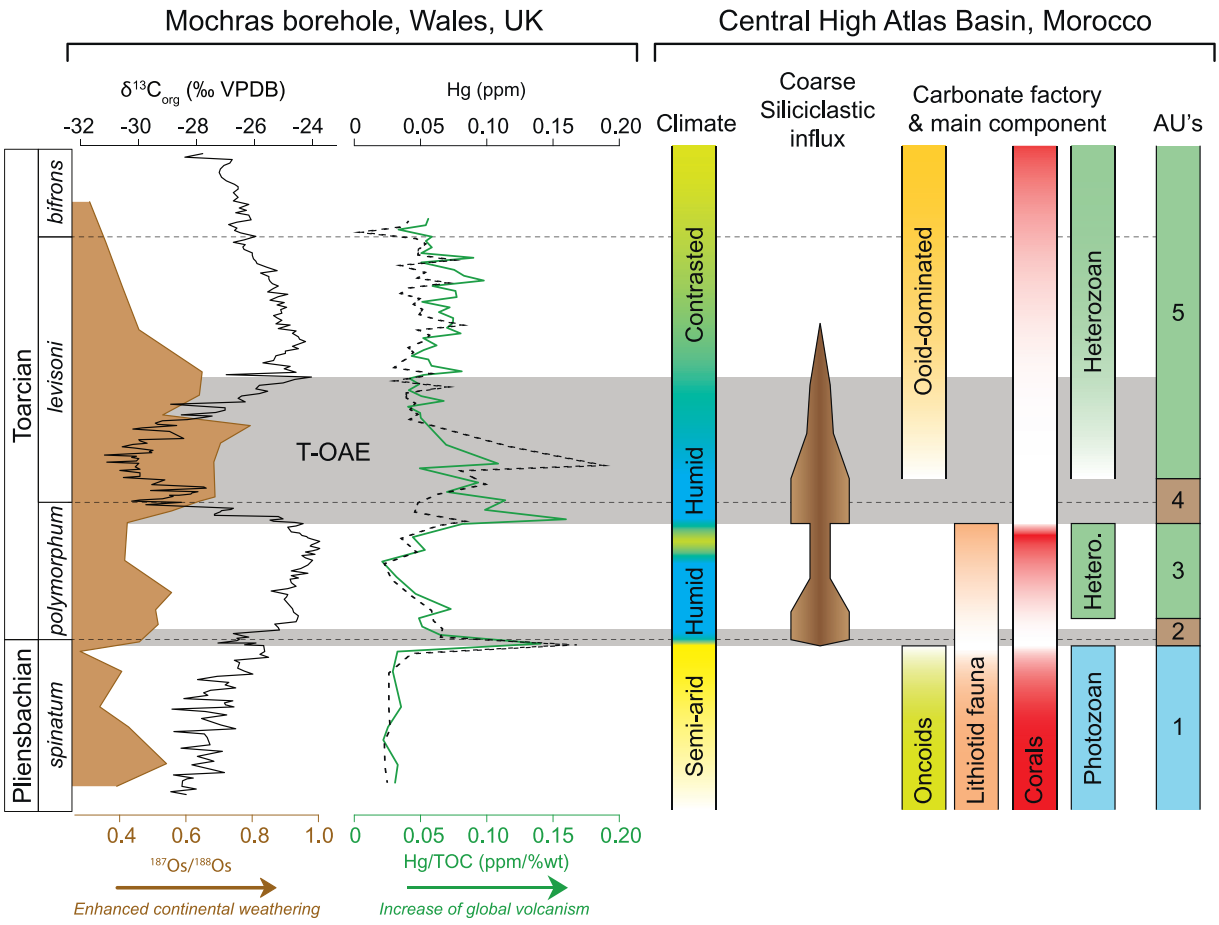

Fig. 9. Summary of environmental and neritic carbonate production changes observed in the central High Atlas during the latest Pliensbachian–middle Toarcian. The timing of these events is compared to the Mochras borehole dataset (δ13Corg data from Xu et al., 2018; Hg/TOC record from Percival et al., 2015, 2016; 187Os/188Os record from Percival et al., 2016), giving insight about global change in carbon cycle, volcanic activity, and continental weathering rates.

Suan et al., 2010; Krencker et al., 2014), suggesting that seawater temperature was not a main driver for neritic carbonate factory changes in the central High Atlas Basin. After the T-OAE, the central High Atlas Basin did not return to the photozoan-dominated carbonate factory like the one that thrived in the Pliensbachian, although several coral reefs do begin to return in deeper water settings. Instead, the T-OAE marks to onset of the long-term progradation of a heterozoan, ooid-dominated ramp (e.g. Pierre et al., 2010) until the closure of the basin in mid-Jurassic time.

7. Conclusion

In the central High Atlas of Morocco, the upper Pliensbachian–middle Toarcian stratigraphic interval is characterized by the successive development of five different neritic carbonate phases. Each phase corresponds to global environmental perturbations and manifests as a change in either the siliciclastic continental input and/or the main carbonate producers. Herein, we report two episodes of carbonate productivity shutdown: 1) at the Pliensbachian/Toarcian boundary, and 2) at the Polymorphum/Levisoni transition (coincident with the onset of the Toarcian Oceanic Anoxic Event). These two episodes are associated with global faunal turnovers and carbon cycle perturbations as highlighted by $\delta^{13}C$ records from various sites. They also correspond to periods of increased delivery of coarse siliciclastic material into the basin, highlighting the intimate link between carbonate factory crisis and increased continental weathering. Altogether, these observations highlight how climate changes can act as a triggering mechanism for carbonate platform shutdowns.

An important outcome of this study is also to specify that in Morocco and in the NW Tethys, the most severe episode of neritic carbonate factory collapse occurred at the Pliensbachian/Toarcian boundary and not during the T-OAE. This observation questions firstly the role of ocean acidification as a main driver for marine carbonate crises during the early Toarcian in general, since ocean acidification has primarily been hypothesized to have occurred at the onset of the T-OAE. This was probably due to the fact that the Pl/To and the T-OAE were often regarded as a single event most likely because the Polymorphum/Tenuicostatum Zone is commonly condensed in the rock recorded. Secondly, it further reinforces the notion that the T-OAE is inscribed within a broader environmental perturbation initiated at the Pliensbachian/Toarcian boundary. Moreover, it is important to recognize that the biotic responses to these events could be very different in black shale-prone restricted basins versus shallow marine carbonates. These data highlight the need for more research on the Pliensbachian/Toarcian boundary event as well as studies focused on different environments.

This study also documents the overall resilience of neritic carbonate factory in the central High Atlas Basin, which recovers surprisingly quickly after each event. Interestingly, the neritic carbonate factory recovered between the Pliensbachian/Toarcian boundary and the T-OAE under mesotrophic conditions, highlighting that increased marine nutrient levels were not the sole factor behind the neritic carbonate factory crises. Furthermore, it is worth noting that the carbonate crisis associated with the onset of the T-OAE is short-lived in the central High Atlas Basin; by the end of the negative $\delta^{13}C$ shift characterizing the onset of the T-OAE, an ooid-dominated carbonate factory reinitiates,

hence well before the end of the T-OAE geochemical perturbation.

Declaration of competing interest

The authors declare that they have no known competing financial interests or personal relationships that could have appeared to influence the work reported in this paper.

Acknowledgements

This research was financed by the Deutsche Forschungsgemeinschaft (DFG, project n° BO 3655/1-1), Bochum University, Germany, granted to Stéphane Bodin (SB) and the Aarhus Universitets Forskningsfond (grant n° AUFF-E-2015-FLS-8-77), Aarhus University, Denmark, granted to Stéphane Bodin (SB), as well as the NSF EAR Grant #1848393, The University of Texas Austin, United States, granted to Rowan Martindale (RCM). Alexis Nutz, Laura Henkel, Martin Hönig, Tim Kothe, Nick Ettinger, Hannah Brame, Sean Kacur, and Mickaël Charpentier are thanked for their help during field expeditions and for laboratory work at Bochum and Aarhus. We are grateful to Editor Alessandra Negri and Jean-François Deconinck and an anonymous reviewer for their constructive comments and suggestions on this manuscript. The authors would like to dedicate this study to the memory of the late Professor Karl Föllmi.

Appendix A. Supplementary data

Supplementary data to this article can be found online at https://doi.org/10.1016/j.earscirev.2020.103254.

References

Ait-Itto, F.Z., Martinez, M., Price, G.D., Addi, A.A., 2018. Synchronization of the astronomical time scales in the Early Toarcian: a link between anoxia, carbon-cycle perturbation, mass extinction and volcanism. Earth Planet. Sci. Lett. 493, 1–11.

Alméras, Y., 2000. Les brachiopodes liasiques des Pyrénées: paléontologie, biostratigraphie, paléobiogéographie et paléoenvironnements. In: Faure, P. (Ed.), Laboratoire de géologie sédimentaire et paléontologie. Université Paul Sabatier, Toulouse.

Al-Suwaidi, A.H., Angelozzi, G.N., Baudin, F., Damborenea, S.E., Hesselbo, S.P., Jenkyns, H.C., Mancenido, M.O., Riccardi, A.C., 2010. First record of the Early Toarcian oceanic anoxic event from the Southern Hemisphere, Neuquen Basin, Argentina. J. Geol. Soc. 167, 633–636.

Baeza-Carratalá, J.F., Joral, F.G., Tent-Manclús, J.E., 2011. Biostratigraphy and paleobiogeographic affinities of the Jurassic brachiopod assemblages from Sierra Espuña (Malaguide Complex, Internal Betic Zones, Spain). J. Iber. Geol. 37, 137–151.

Baghli, H., Mattioli, E., Spangenberg, J.E., Bensalah, M., Arnaud-Godet, F., Pittet, B., Suan, G., 2020. Early Jurassic climatic trends in the south-Tethyan margin. Gondwana Res. 77, 67–81.

Bailey, T.R., Rosenthal, Y., McArthur, J.M., van de Schootbrugge, B., Thirlwall, M.F., 2003. Paleoceanographic changes of the Late Pliensbachian-Early Toarcian interval: a possible link to the genesis of an Oceanic Anoxic Event. Earth Planet. Sci. Lett. 212, 307–320.

Ball, M.M., Shinn, E.A., Stockman, K.W., 1967. The geologic effects of Hurricane Donna in south Florida. J. Geol. 75, 583–597.

Baroni, I.R., Pohl, A., van Helmond, N.A.G.M., Papadomanolaki, N.M., Coe, A.L., Cohen, A.S., van de Schootbrugge, B., Donnadieu, Y., Slomp, C.P., 2018. Ocean Circulation in the Toarcian (Early Jurassic): a key control on deoxygenation and carbon burial on the European shelf. Paleoceanogr. Paleoclimatol. 33, 994–1012.

Barth, G., Pieńkowski, G., Zimmermann, J., Franz, M., Kuhlmann, G., 2018. Palaeogeographical evolution of the Lower Jurassic: high-resolution biostratigraphy and sequence stratigraphy in the Central European Basin. Geol. Soc. Lond., Spec. Publ. 469, 341.

Bassoulet, J.P., Elmi, S., Poisson, A., Ricou, L.E., Cecca, F., Bellion, Y., Guiraud, R., Baudin, F., 1993. Mid Toarcian (184 to 182 Ma). In: Dercourt, J., Ricou, L.E., Vrielynck, B. (Eds.), Atlas Tethys Palaeoenvironmental Maps, pp. 63–80.

Blomeier, D.P.G., Reijmer, J.J.G., 1999. Drowning of a lower Jurassic carbonate platform: Jbel Bou Dahar, High Atlas, Morocco. Facies 41, 81–110.

Bodin, S., Godet, A., Föllmi, K.B., Vermeulen, J., Arnaud, H., Strasser, A., Fiet, N., Adatte, T., 2006. The late Hauterivian Faraoni oceanic anoxic event in the western Tethys: evidence from phosphorus burial rates. Palaeogeogr. Palaeoclimatol. Palaeoecol. 235, 245–264.

Bodin, S., Godet, A., Matera, V., Steinmann, P., Vermeulen, J., Gardin, S., Adatte, T., Coccioni, R., Föllmi, K.B., 2007. Enrichment of redox-sensitive trace metals (U, V, Mo, As) associated with the late Hauterivian Faraoni oceanic anoxic event. Int. J. Earth Sci. 96, 327–341.

Bodin, S., Mattioli, E., Frohlich, S., Marshall, J.D., Boutib, L., Lahsini, S., Redfern, J., 2010. Toarcian carbon isotope shifts and nutrient changes from the Northern margin of Gondwana (High Atlas, Morocco, Jurassic): palaeoenvironmental implications. Palaeogeogr. Palaeoclimatol. Palaeoecol. 297, 377–390.

Bodin, S., Frohlich, S., Boutib, L., Lahsini, S., Redfern, J., 2011. Early Toarcian source-rock potential in the central high atlas basin (Central Morocco): regional distribution and depositional model. J. Pet. Geol. 34, 345–363.

Bodin, S., Krencker, F.N., Kothe, T., Hoffmann, R., Mattioli, E., Heimhofer, U., Kabiri, L., 2016. Perturbation of the carbon cycle during the late Pliensbachian – early Toarcian: new insight from high-resolution carbon isotope records in Morocco. J. Afr. Earth Sci. 116, 89–104.

Bodin, S., Honig, M.R., Krencker, F.N., Danisch, J., Kabiri, L., 2017. Neritic carbonate crisis during the Early Bajocian: divergent responses to a global environmental perturbation. Palaeogeogr. Palaeoclimatol. Palaeoecol. 468, 184–199.

Bouchouata, A., Canerot, J., Abdellatif, S., Almeras, Y., 1995. Stratigraphie séquentielle et évolution géodynamique du Jurassique dans la région de Talmest-Tazoult (Haut Atlas central, Maroc); Jurassic sequence stratigraphy and geodynamic evolution in the Talmest-Tazoult area (Central High Atlas, Morocco). In: Comptes rendus de l'Académie des sciences. Série 2. Sciences de la terre et des planètes 320, pp. 749–756.

Boulila, S., Galbrun, B., Sadki, D., Gardin, S., Bartolini, A., 2019. Constraints on the duration of the early Toarcian T-OAE and evidence for carbon-reservoir change from the High Atlas (Morocco). Glob. Planet. Chang. 175, 113–128.

Brame, H.-M.R., Martindale, R.C., Ettinger, N.P., Debeljak, I., Vasseur, R., Lathuilière, B., Kabiri, L., Bodin, S., 2019. Stratigraphic distribution and paleoecological significance of Early Jurassic (Pliensbachian-Toarcian) lithiotid-coral reefal deposits from the Central High Atlas of Morocco. Palaeogeogr. Palaeoclimatol. Palaeoecol. 514, 813–837.

Brandano, M., Mateu-Vicens, G., Gianfagna, A., Corda, L., Billi, A., Quaresima, S., Simonetti, A., 2009. Hardground development and drowning of a Miocene carbonate ramp (Latium-Abruzzi): from tectonic to paleoclimate. J. Mediterr. Earth Sci. 1, 47–56.

Brazier, J.M., Suan, G., Tacail, T., Simon, L., Martin, J.E., Mattioli, E., Balter, V., 2015. Calcium isotope evidence for dramatic increase of continental weathering during the Toarcian oceanic anoxic event (Early Jurassic). Earth Planet. Sci. Lett. 411, 164–176.

Caruthers, A.H., Grocke, D.R., Smith, P.L., 2011. The significance of an Early Jurassic (Toarcian) carbon-isotope excursion in Haida Gwaii (Queen Charlotte Islands), British Columbia, Canada. Earth Planet. Sci. Lett. 307, 19–26.

Caruthers, A.H., Smith, P.L., Grocke, D.R., 2013. The Pliensbachian-Toarcian (Early Jurassic) extinction, a global multi-phased event. Palaeogeogr. Palaeoclimatol. Palaeoecol. 386, 104–118.

Caruthers, A.H., Smith, P.L., Gröcke, D.R., 2014. The Pliensbachian–Toarcian (Early Jurassic) Extinction: a north American Perspective. Geol. Soc. Am. Spec. Pap. 505 (September), 225–243. https://doi.org/10.1130/2014.2505(11).

Cecca, F., Macchioni, F., 2004. The two Early Toarcian (Early Jurassic) extinction events in ammonoids. Lethaia 37, 35–56.

Clemence, M.E., 2014. Pattern and timing of the Early Jurassic calcareous nannofossil crisis (Retracted article. See vol. 435, pg. 283, 2015). Palaeogeogr. Palaeoclimatol. Palaeoecol. 411, 56–64.

Cohen, A.S., Coe, A.L., Harding, S.M., Schwark, L., 2004. Osmium isotope evidence for the regulation of atmospheric CO2 by continental weathering. Geology 32, 157–160.

Comas Rengifo, M.J., Duarte, L.V., García Joral, F., Goy, A., 2013. The brachiopod record in the Lower Toarcian (Jurassic) of the Rabaçal-Condeixa region (Portugal): stratigraphic distribution and paleobiogeography. Comun. Geol. 100, 37–42.

Cope, J.C.W., Getty, T.A., Howarth, M.K., Morton, N., Torrens, H.S., Duff, K.L., Parsons, C.F., Wimbledon, W.A., Wright, J.K., 1980. A correlation of Jurassic rocks in British Isles; Corrélation du Jurassique des îles Britanniques.

Črne, A.E., GoriČan, S., 2008. The Dinaric Carbonate Platform margin in the Early Jurassic: a comparison between successions in Slovenia and Montenegro. Boll. Soc. Geol. Ital. 127, 389–405.

Danise, S., Clemence, M.E., Price, G.D., Murphy, D.P., Gomez, J.J., Twitchett, R.J., 2019. Stratigraphic and environmental control on marine benthic community change through the early Toarcian extinction event (Iberian Range, Spain). Palaeogeogr. Palaeoclimatol. Palaeoecol. 524, 183–200.

Deconinck, J.-F., Gómez, J.J., Baudin, F., Biscay, H., Bruneau, L., Cocquerez, T., Mathieu, O., Pellenard, P., Santoni, A.-L., 2020. Diagenetic and environmental control of the clay mineralogy, organic matter and stable isotopes (C, O) of Jurassic (Pliensbachian-lowermost Toarcian) sediments of the Rodiles section (Asturian Basin, Northern Spain). Mar. Pet. Geol. 115, 104286.

Dera, G., Donnadieu, Y., 2012. Modeling evidences for global warming, Arctic seawater freshening, and sluggish oceanic circulation during the Early Toarcian anoxic event. Paleoceanography 27, PA2211.

Dera, G., Pucéat, E., Pellenard, P., Neige, P., Delsate, D., Joachimski, M.M., Reisberg, L., Martinez, M., 2009a. Water mass exchange and variations in seawater temperature in the NW Tethys during the Early Jurassic: evidence from neodymium and oxygen isotopes of fish teeth and belemnites. Earth Planet. Sci. Lett. 286, 198–207.

Dera, G., Pellenard, P., Neige, P., Deconinck, J.-F., Pucéat, E., Dommergues, J.-L., 2009b. Distribution of clay minerals in Early Jurassic Peritethyan seas: palaeoclimatic significance inferred from multiproxy comparisons. Palaeogeogr. Palaeoclimatol. Palaeoecol. 271, 39–51.

Dera, G., Neige, P., Dommergues, J.L., Fara, E., Laffont, R., Pellenard, P., 2010. High-resolution dynamics of Early Jurassic marine extinctions: the case of Pliensbachian-Toarcian ammonites (Cephalopoda). J. Geol. Soc. 167, 21–33.

Dera, G., Brigaud, B., Monna, F., Laffont, R., Puceat, E., Deconinck, J.F., Pellenard, P., Joachimski, M.M., Durlet, C., 2011a. Climatic ups and downs in a disturbed Jurassic world. Geology 39, 215–218.

Dera, G., Neige, P., Dommergues, J.L., Brayard, A., 2011b. Ammonite paleobiogeography during the Pliensbachian-Toarcian crisis (Early Jurassic) reflecting paleoclimate, eustasy, and extinctions. Glob. Planet. Chang. 78, 92–105.
Diaz, M.R., Eberli, G.P., 2019. Decoding the mechanism of formation in marine ooids: a review. Earth Sci. Rev. 190, 536–556.
Donnadieu, Y., Dromart, G., Godderis, Y., Pucéat, E., Brigaud, B., Dera, G., Dumas, C., Olivier, N., 2011. A mechanism for brief glacial episodes in the Mesozoic greenhouse. Paleoceanography 26.
Dromart, G., Allemand, P., García, J.P., Robin, C., 1996. Cyclic fluctuation of carbonate production through the Jurassic along a Burgundy-Ardeche cross-section, eastern France. Bull. Soc. Geol. France 167, 423–433.
Drzewiecki, P.A., Simo, J.A.T., 1997. Carbonate platform drowning and oceanic anoxic events on a Mid-cretaceous carbonate platform, South-Central Pyrenees, Spain. J. Sediment. Res. 67 (4), 698–714.
Du Dresnay, R., 1971. Extension et développement des phénomènes récifaux Jurassiques dans le domaine atlasique marocain, particulièrement au lias moyen. Bull. Soc. Geol. France (13), 46–56.
Dunhill, A.M., Foster, W.J., Azaele, S., Sciberras, J., Twitchett, R.J., 2018. Modelling determinants of extinction across two Mesozoic hyperthermal events. Proc. R. Soc. Lond. B Biol. Sci. 285, 20180404.
Eichenseer, K., Balthasar, U., Smart, C.W., Stander, J., Haaga, K.A., Kiessling, W., 2019. Jurassic shift from abiotic to biotic control on marine ecological success. Nat. Geosci. 12, 638–642.
Erba, E., 2004. Calcareous nannofossils and Mesozoic oceanic anoxic events. Mar. Micropaleontol. 52, 85–106.
Ettaki, M., Chellaï, E.H., 2005. Le Toarcien inférieur du Haut Atlas de Todrha–Dadès (Maroc): sédimentologie et lithostratigraphie. Compt. Rendus Geosci. 337, 814–823.
Ettaki, M., Chellaï, E.H., Milhi, A., Sadki, D., Boudchiche, L., 2000. Le passage Lias moyen–Lias supérieur dans la région de Todrha-Dadès: événements bio-sédimentaires et géodynamiques (Haut Atlas central, Maroc). C. R. Acad. Sci. Ser. IIA Earth Planet. Sci. 331, 667–674.
Ettinger, N.P., Larson, T.E., Kerans, C., Thibodeau, A., Hattori, K.E., Kacur, S.M., Martindale, R.C., 2020. Ocean acidification and photic-zone anoxia at the Toarcian Oceanic Anoxic Event: insights from the Adriatic Carbonate Platform. Sedimentology submitted.
Fantasia, A., Föllmi, K.B., Adatte, T., Bernárdez, E., Spangenberg, J.E., Mattioli, E., 2018a. The Toarcian Oceanic Anoxic Event in southwestern Gondwana: an example from the Andean Basin, northern Chile. J. Geol. Soc. 175, 883–902.
Fantasia, A., Föllmi, K.B., Adatte, T., Spangenberg, J.E., Montero-Serrano, J.C., 2018b. The Early Toarcian oceanic anoxic event: Paleoenvironmental and paleoclimatic change across the Alpine Tethys (Switzerland). Glob. Planet. Chang. 162, 53–68.
Fantasia, A., Adatte, T., Spangenberg, J.E., Font, E., Duarte, L.V., Föllmi, K.B., 2019a. Global versus local processes during the Pliensbachian-Toarcian transition at the Peniche GSSP, Portugal: a multi-proxy record. Earth Sci. Rev. 198.
Fantasia, A., Föllmi, K.B., Adatte, T., Spangenberg, J.E., Mattioli, E., 2019b. Expression of the Toarcian Oceanic Anoxic Event: new insights from a Swiss transect. Sedimentology 66, 262–284.
Föllmi, K.B., Godet, A., Bodin, S., Linder, P., 2006. Interactions between environmental change and shallow water carbonate buildup along the northern Tethyan margin and their impact on the Early Cretaceous carbon isotope record. Paleoceanography 21.
Föllmi, K.B., Bôle, M., Jammet, N., Froidevaux, P., Godet, A., Bodin, S., Adatte, T., Matera, V., Fleitmann, D., Spangenberg, J.E., 2012. Bridging the Faraoni and Selli oceanic anoxic events: late Hauterivian to early Aptian dysaerobic to anaerobic phases in the Tethys. Clim. Past 8, 171–189.
Fraser, N.M., Bottjer, D.J., Fischer, A.G., 2004. Dissecting "Lithiotis" bivalves: Implications for the Early Jurassic reef eclipse. Palaios 19, 51–67.
French, K.L., Sepulveda, J., Trabucho-Alexandre, J., Grocke, D.R., Summons, R.E., 2014. Organic geochemistry of the early Toarcian oceanic anoxic event in Hawsker Bottoms, Yorkshire, England. Earth Planet. Sci. Lett. 390, 116–127.
Frizon de Lamotte, D., Zizi, M., Missenard, Y., Hafid, M., Azzouzi, M.E., Maury, R.C., Charrière, A., Taki, Z., Benammi, M., Michard, A., 2008. The atlas system. In: Michard, A., Saddiqi, O., Chalouan, A., Lamotte, D.F.d (Eds.), Continental Evolution: The Geology of Morocco: Structure, Stratigraphy, and Tectonics of the Africa-Atlantic-Mediterranean Triple Junction. Springer Berlin Heidelberg, Berlin, Heidelberg, pp. 133–202.
Ghorbal, B., Bertotti, G., Foeken, J., Andriessen, P., 2008. Unexpected Jurassic to Neogene vertical movements in 'stable' parts of NW Africa revealed by low temperature geochronology. Terra Nova 20, 355–363.
Godet, A., 2013. Drowning unconformities: Palaeoenvironmental significance and involvement of global processes. Sediment. Geol. 293, 45–66.
Godet, A., Föllmi, K.B., Spangenberg, J.E., Bodin, S., Vermeulen, J., Adatte, T., Bonvallet, L., Arnaud, H., 2013. Deciphering the message of Early cretaceous drowning surfaces from the Helvetic Alps: what can be learnt from platform to basin correlations? Sedimentology 60, 152–173.
Gomez, J.J., Goy, A., Canales, M.L., 2008. Seawater temperature and carbon isotope variations in belemnites linked to mass extinction during the Toarcian (Early Jurassic) in Central and Northern Spain. Comparison with other European sections. Palaeogeogr. Palaeoclimatol. Palaeoecol. 258, 28–58.
Grasby, Them, Chen, Yin, Ardakani, 2019. Mercury as a proxy for volcanic emissions in the geologic record. Earth-Sci Rev 196, 102880.
Greene, S.E., Martindale, R.C., Ritterbush, K.A., Bottjer, D.J., Corsetti, F.A., Berelson, W.M., 2012. Recognising Ocean acidification in deep time: an evaluation of the evidence for acidification across the Triassic-Jurassic boundary. Earth Sci. Rev. 113, 72–93.
Gröcke, D.R., Rimmer, S.M., Yoksoulian, L.E., Cairncross, B., Tsikos, H., van Hunen, J., 2009. No evidence for thermogenic methane release in coal from the Karoo-Ferrar large igneous province. Earth Planet. Sci. Lett. 277, 204–212.
Gröcke, D.R., Hori, R.S., Trabucho-Alexandre, J., Kemp, D.B., Schwark, L., 2011. An open ocean record of the Toarcian oceanic anoxic event. Solid Earth 2, 245–257.
Guex, J., Bartolini, A., Spangenberg, J., Vicente, J.C., Schaltegger, U., 2012. Ammonoid multi-extinction crises during the Late Pliensbachian–Toarcian and carbon cycle instabilities. Solid Earth Discussion. 2012, 1205–1228.
Hadri, M., 1997. Carte géologique du Maroc 1:100 000. NH-30-XIX-4, Tinejdad/Royaume du Maroc. In: (Rabat), E.d.S.G.d.M (Ed.), Ministère de l'Energie et des Mines, Direction de la Géologie, Rabat, pp. 1 carte: en couleur; 58 x 50 cm, sur 51 flle 95 x 99 cm.
Halfar, J., Godinez-Orta, L., Mutti, M., Valdez-Holguin, J.E., Borges, J.M., 2006. Carbonates calibrated against oceanographic parameters along a latitudinal transect in the Gulf of California, Mexico. Sedimentology 53, 297–320.
Hallam, A., 1997. Estimates of the amount and rate of sea-level change across the Rhaetian-Hettangian and Pliensbachian-Toarcian boundaries (latest Triassic to early Jurassic). J. Geol. Soc. 154, 773–779.
Hallock, P., Schlager, W., 1986. Nutrient excess and the demise of coral reefs and carbonate platforms. Palaios 1, 389–398.
Han, Z., Hu, X., Kemp, D.B., Li, J., 2018. Carbonate-platform response to the Toarcian Oceanic Anoxic Event in the southern hemisphere: implications for climatic change and biotic platform demise. Earth Planet. Sci. Lett. 489, 59–71.
Harries, P.J., Little, C.T.S., 1999. The early Toarcian (Early Jurassic) and the Cenomanian-Turonian (Late Cretaceous) mass extinctions: similarities and contrasts. Palaeogeogr. Palaeoclimatol. Palaeoecol. 154, 39–66.
Hermoso, M., Pellenard, P., 2014. Continental weathering and climatic changes inferred from clay mineralogy and paired carbon isotopes across the early to middle Toarcian in the Paris Basin. Palaeogeogr. Palaeoclimatol. Palaeoecol. 399, 385–393.
Hermoso, M., Minoletti, F., Rickaby, R.E.M., Hesselbo, S.P., Baudin, F., Jenkyns, H.C., 2012. Dynamics of a stepped carbon-isotope excursion: ultra high-resolution study of Early Toarcian environmental change. Earth Planet. Sci. Lett. 319–320, 45–54.
Hermoso, M., Minoletti, F., Pellenard, P., 2013. Black shale deposition during Toarcian super-greenhouse driven by sea level. Clim. Past 9, 2703–2712.
Hesselbo, Gröcke, Jenkyns, Bjerrum, Farrimond, Bell, Green, 2000. Massive dissociation of gas hydrate during a Jurassic oceanic anoxic event. Nature 406, 392–395. https://doi.org/10.1038/35019044.
Hesselbo, S.P., Jenkyns, H.C., Duarte, L.V., Oliveira, L.C.V., 2007. Carbon-isotope record of the Early Jurassic (Toarcian) Oceanic Anoxic Event from fossil wood and marine carbonate (Lusitanian Basin, Portugal). Earth Planet. Sci. Lett. 253, 455–470.
Hönisch, B., Ridgwell, A., Schmidt, D.N., Thomas, E., Gibbs, S.J., Sluijs, A., Zeebe, R., Kump, L., Martindale, R.C., Greene, S.E., Kiessling, W., Ries, J., Zachos, J.C., Royer, D.L., Barker, S., Marchitto, T.M., Moyer, R., Pelejero, C., Ziveri, P., Foster, G.L., Williams, B., 2012. The Geological record of ocean acidification. Science 335, 1058.
Hueter, A., Huck, S., Bodin, S., Heimhofer, U., Weyer, S., Jochum, K.P., Immenhauser, A., 2019. Central tethyan platform-top hypoxia during oceanic anoxic event 1a. Clim. Past 15, 1327–1344.
Ibouh, H., Bchari, F.E., Bouabdelli, M., Souhel, A., Youbi, N., 2001. L'accident Tizal-Azourki Haut Atlas central du Maroc: déformations synsédimentaires Liasiques en extension et conséquences du serrage Atlasique. Estud. Geol. 57, 15–30.
Ikeda, M., Hori, R.S., Ikehara, M., Miyashita, R., Chino, M., Yamada, K., 2018. Carbon cycle dynamics linked with Karoo-Ferrar volcanism and astronomical cycles during Pliensbachian-Toarcian (Early Jurassic). Glob. Planet. Chang. 170, 163–171.
Immenhauser, A., 2005. High-rate Sea-level change during the Mesozoic: new approaches to an old problem. Sediment. Geol. 175, 277–296.
Jenkyns, H.C., 1988. The early Toarcian (Jurassic) anoxic event; stratigraphic, sedimentary and geochemical evidence. Am. J. Sci. 288 (2), 101–151.
Jenkyns, H.C., 2010. Geochemistry of oceanic anoxic events. Geochem. Geophys. Geosyst. 11.
Joral, F.G., Gomez, J.J., Goy, A., 2011. Mass extinction and recovery of the early Toarcian (Early Jurassic) brachiopods linked to climate change in Northern and Central Spain. Palaeogeogr. Palaeoclimatol. Palaeoecol. 302, 367–380.
Jossen, J.-A., 1988. Carte géologique de Zawiat Ahançal. 1/100.000. Notes et Mémoires du Service Géologique du Maroc, Rabat.
Jourdan, F., Feraud, G., Bertrand, H., Watkeys, M.K., Renne, P.R., 2008. The (40)Ar/(39)Ar ages of the sill complex of the Karoo large igneous province: implications for the Pliensbachian-Toarcian climate change. Geochem. Geophys. Geosyst. 9.
Kemp, D.B., Coe, A.L., Cohen, A.S., Weedon, G.P., 2011. Astronomical forcing and chronology of the early Toarcian (Early Jurassic) oceanic anoxic event in Yorkshire, UK. Paleoceanography 26.
Kiessling, W., Simpson, C., 2011. On the potential for ocean acidification to be a general cause of ancient reef crises. Glob. Chang. Biol. 17, 56–67.
Korte, C., Hesselbo, S.P., Ullmann, C.V., Dietl, G., Ruhl, M., Schweigert, G., Thibault, N., 2015. Jurassic climate mode governed by ocean gateway. Nat. Commun. 6.
Krencker, F.N., Bodin, S., Hoffmann, R., Suan, G., Mattioli, E., Kabiri, L., Föllmi, K.B., Immenhauser, A., 2014. The middle Toarcian cold snap: trigger of mass extinction and carbonate factory demise. Glob. Planet. Chang. 117, 64–78.
Krencker, F.N., Bodin, S., Suan, G., Heimhofer, U., Kabiri, L., Immenhauser, A., 2015. Toarcian extreme warmth led to tropical cyclone intensification. Earth Planet. Sci. Lett. 425, 120–130.
Krencker, F.N., Lindstrom, S., Bodin, S., 2019. A major sea-level drop briefly precedes the Toarcian oceanic anoxic event: implication for Early Jurassic climate and carbon cycle. Sci. Rep. 9.
Lachkar, N., Guiraud, M., El Harfi, A., Dommergues, J.L., Dera, G., Durlet, C., 2009. Early Jurassic normal faulting in a carbonate extensional basin: characterization of tectonically driven platform drowning (High Atlas rift, Morocco). J. Geol. Soc. 166, 413–430.
Laville, E., Pique, A., Amrhar, M., Charroud, M., 2004. A restatement of the Mesozoic

Atlasic Rifting (Morocco). J. Afr. Earth Sci. 38, 145–153.
Leonide, P., Floquet, M., Durlet, C., Baudin, F., Pittet, B., Lecuyer, C., 2012. Drowning of a carbonate platform as a precursor stage of the Early Toarcian global anoxic event (Southern Provence sub-Basin, South-east France). Sedimentology 59, 156–184.
Lepretre, R., Missenard, Y., Barbarand, J., Gautheron, C., Jouvie, I., Saddiqi, O., 2018. Polyphased inversions of an intracontinental rift: case study of the Marrakech High Atlas, Morocco. Tectonics 37, 818–841.
Little, C.T.S., Benton, M.J., 1995. Early Jurassic mass extinction – a global long-term event. Geology 23, 495–498.
Littler, K., Hesselbo, S.P., Jenkyns, H.C., 2010. A carbon-isotope perturbation at the Pliensbachian-Toarcian boundary: evidence from the Lias Group, NE England. Geol. Mag. 147, 181–192.
Mallin, M.A., Corbett, C.A., 2006. How hurricane attributes determine the extent of environmental effects: multiple hurricanes and different coastal systems. Estuar. Coasts 29, 1046–1061.
Malusa, M.G., Polino, R., Feroni, A.C., Ellero, A., Ottria, G., Baidder, L., Musumeci, G., 2007. Post-Variscan tectonics in eastern Anti-Atlas (Morocco). Terra Nova 19, 481–489.
Martindale, R.C., Aberhan, M., 2017. Response of macrobenthic communities to the Toarcian Oceanic Anoxic Event in northeastern Panthalassa (Ya Ha Tinda, Alberta, Canada). Palaeogeogr. Palaeoclimatol. Palaeoecol. 478, 103–120.
Martinez, M., Krencker, F.N., Mattioli, E., Bodin, S., 2017. Orbital chronology of the Pliensbachian – Toarcian transition from the Central High Atlas Basin (Morocco). Newsl. Stratigr. 50, 47–69.
Mattioli, E., Pittet, B., 2004. Spatial and temporal distribution of calcareous nannofossils along a proximal-distal transect in the Lower Jurassic of the Umbria-Marche Basin (central Italy). Palaeogeogr. Palaeoclimatol. Palaeoecol. 205, 295–316.
Mattioli, E., Pittet, B., Suan, G., Mailliot, S., 2008. Calcareous nannoplankton changes across the early Toarcian oceanic anoxic event in the western Tethys. Paleoceanography 23.
Mattioli, E., Pittet, B., Petitpierre, L., Mailliot, S., 2009. Dramatic decrease of pelagic carbonate production by nannoplankton across the Early Toarcian anoxic event (T-OAE). Glob. Planet. Chang. 65, 134–145.
McArthur, J.M., Donovan, D.T., Thirlwall, M.F., Fouke, B.W., Mattey, D., 2000. Strontium isotope profile of the early Toarcian (Jurassic) oceanic anoxic event, the duration of ammonite biozones, and belemnite palaeotemperatures. Earth Planet. Sci. Lett. 179, 269–285.
McElwain, J.C., Wade-Murphy, J., Hesselbo, S.P., 2005. Changes in carbon dioxide during an oceanic anoxic event linked to intrusion into Gondwana coals. Nature 435, 479–482.
Mehdi, M., Neuweiler, F., Wilmsen, M., 2003. Lower Liassic Formations of the Central High-Atlas near Rich (Morocco): lithostratigraphic specification and basin evolution. Bull. Soc. Geol. France 174, 227–242.
Michel, J., Laugie, M., Pohl, A., Lanteaume, C., Masse, J.P., Donnadieu, Y., Borgomano, J., 2019. Marine carbonate factories: a global model of carbonate platform distribution. Int. J. Earth Sci. 108, 1773–1792.
Montero-Serrano, J.C., Foellmi, K.B., Adatte, T., Spangenberg, J.E., Tribovillard, N., Fantasia, A., Suan, G., 2015. Continental weathering and redox conditions during the early Toarcian Oceanic Anoxic Event in the northwestern Tethys: insight from the Posidonia Shale section in the Swiss Jura Mountains. Palaeogeogr. Palaeoclimatol. Palaeoecol. 429, 83–99.
Moragas, M., Vergés, J., Saura, E., Martín-Martín, J.-D., Messager, G., Merino-Tomé, Ó., Suárez-Ruiz, I., Razin, P., Grélaud, C., Malaval, M., Joussiaume, R., Hunt, D.W., 2018. Jurassic rifting to post-rift subsidence analysis in the Central High Atlas and its relation to salt diapirism. Basin Res. 30, 336–362.
Mutti, M., Hallock, P., 2003. Carbonate systems along nutrient and temperature gradients: some sedimentological and geochemical constraints. Int. J. Earth Sci. 92, 465–475.
Mutti, M., Bernoulli, D., Stille, P., 1997. Temperate carbonate platform drowning linked to Miocene oceanographic events: Maiella platform margin, Italy. Terra Nova 9, 122–125.
Newton, R.J., Reeves, E.P., Kafousia, N., Wignall, P.B., Bottrell, S.H., Sha, J.G., 2011. Low marine sulfate concentrations and the isolation of the European epicontinental sea during the Early Jurassic. Geology 39, 7–10.
Ogg, J.G., Ogg, G.M., Gradstein, F.M., 2016. A Concise Geologic Time Scale 2016. Elsevier, Oxford.
Oukassou, M., Saddiqi, O., Barbarand, J., Sebti, S., Baidder, L., Michard, A., 2013. Post-Variscan exhumation of the Central Anti-Atlas (Morocco) constrained by zircon and apatite fission-track thermochronology. Terra Nova 25, 151–159.
Paerl, H.W., Bales, J.D., Ausley, L.W., Buzzelli, C.P., Crowder, L.B., Eby, L.A., Fear, J.M., Go, M., Peierls, B.L., Richardson, T.L., Ramus, J.S., 2001. Ecosystem impacts of three sequential hurricanes (Dennis, Floyd, and Irene) on the United States' largest lagoonal estuary, Pamlico Sound, NC. Proc. Natl. Acad. Sci. 98, 5655.
Percival, L.M.E., Witt, M.L.I., Mather, T.A., Hermoso, M., Jenkyns, H.C., Hesselbo, S.P., Al-Suwaidi, A.H., Storm, M.S., Xu, W., Ruhl, M., 2015. Globally enhanced mercury deposition during the end-Pliensbachian extinction and Toarcian OAE: a link to the Karoo-Ferrar large Igneous Province. Earth Planet. Sci. Lett. 428, 267–280.
Percival, L.M.E., Cohen, A.S., Davies, M.K., Dickson, A.J., Hesselbo, S.P., Jenkyns, H.C., Leng, M.J., Mather, T.A., Storm, M.S., Xu, W., 2016. Osmium isotope evidence for two pulses of increased continental weathering linked to Early Jurassic volcanism and climate change. Geology 44, 759–762.
Peti, L., Thibault, N., 2017. Abundance and size changes in the calcareous nannofossil Schizosphaerella – relation to sea-level, the carbonate factory and palaeoenvironmental change from the Sinemurian to earliest Toarcian of the Paris Basin. Palaeogeogr. Palaeoclimatol. Palaeoecol. 485, 271–282.
Piazza, V., Ullmann, C.V., Aberhan, M., 2020. Temperature-related body size change of marine benthic macroinvertebrates across the Early Toarcian Anoxic Event. Sci. Rep. 10, 4675.
Pierre, Durlet, Razin, Chellai, 2010. Spatial and temporal distribution of ooids along a Jurassic carbonate ramp: Amellago outcrop transect, High-Atlas, Morocco. Geological Society, London, Special Publications 329, 65.
Pittet, B., Suan, G., Lenoir, F., Duarte, L.V., Mattioli, E., 2014. Carbon isotope evidence for sedimentary discontinuities in the lower Toarcian of the Lusitanian Basin (Portugal): sea level change at the onset of the Oceanic Anoxic Event. Sediment. Geol. 303, 1–14.
Quiquerez, A., Allemand, P., Dromart, G., Garcia, J.-P., 2004. Impact of storms on mixed carbonate and siliciclastic shelves: insights from combined diffusive and fluid-flow transport stratigraphic forward model. Basin Res. 16, 431–449.
Raiswell, R., 1988. Evidence for surface reaction-controlled growth of carbonate concretions in shales. Sedimentology 35, 571–575.
Rengifo, M., LV, D., FF, F., FG, J., A, G., RB, R., 2015. Latest Pliensbachian–Early Toarcian brachiopod assemblages from the Peniche section (Portugal) and their correlation. Int. Union Geol. Sci. 38, 2–8.
Reolid, M., Copestake, P., Johnson, B., 2019. Foraminiferal assemblages, extinctions and appearances associated with the Early Toarcian Oceanic Anoxic Event in the Llanbedr (Mochras Farm) Borehole, Cardigan Bay Basin, United Kingdom. Palaeogeogr. Palaeoclimatol. Palaeoecol. 532, 109277.
Riquier, L., Tribovillard, N., Averbuch, O., Devleeschouwer, X., Riboulleau, A., 2006. The Late Frasnian Kellwasser horizons of the Harz Mountains (Germany): two oxygen-deficient periods resulting from different mechanisms. Chem. Geol. 233, 137–155.
Röhl, H.-J., Schmid-Röhl, A., Oschmann, W., Frimmel, A., Schwark, L., 2001. The Posidonia Shale (Lower Toarcian) of SW-Germany: an oxygen-depleted ecosystem controlled by sea level and palaeoclimate. Palaeogeogr. Palaeoclimatol. Palaeoecol. 165, 27–52.
Rosales, I., Quesada, S., Robles, S., 2004. Paleotemperature variations of Early Jurassic seawater recorded in geochemical trends of belemnites from the Basque-Cantabrian basin, northern Spain. Palaeogeogr. Palaeoclimatol. Palaeoecol. 203, 253–275.
Ruebsam, W., Al-Husseini, M., 2020. Calibrating the Early Toarcian (Early Jurassic) with stratigraphic black holes (SBH). Gondwana Res. 82, 317–336.
Ruebsam, W., Mayer, B., Schwark, L., 2019. Cryosphere carbon dynamics control early Toarcian global warming and sea level evolution. Glob. Planet. Chang. 172, 440–453.
Ruebsam, W., Reolid, M., Marok, A., Schwark, L., 2020a. Drivers of benthic extinction during the early Toarcian (Early Jurassic) at the northern Gondwana paleomargin: Implications for paleoceanographic conditions. Earth Sci. Rev. 203, 103117.
Ruebsam, W., Reolid, M., Schwark, L., 2020b. δ13C of terrestrial vegetation records Toarcian CO_2 and climate gradients. Sci. Rep. 10, 117.
Ruiz, G.M.H., Sebti, S., Negro, F., Saddiqi, O., de Lamotte, D.F., Stockli, D., Foeken, J., Stuart, F., Barbarand, J., Schaer, J.P., 2011. From central Atlantic continental rift to Neogene uplift – western Anti-Atlas (Morocco). Terra Nova 23, 35–41.
Sabatino, N., Vlahovic, I., Jenkyns, H.C., Scopelliti, G., Neri, R., Prtoljan, B., Velic, I., 2013. Carbon-isotope record and palaeoenvironmental changes during the early Toarcian oceanic anoxic event in shallow-marine carbonates of the Adriatic Carbonate Platform in Croatia. Geol. Mag. 150, 1085–1102.
Saddiqi, O., El Haimer, F.Z., Michard, A., Barbarand, J., Ruiz, G.M.H., Mansour, E.M., Leturmy, P., de Lamotte, D., 2009. Apatite fission-track analyses on basement granites from south-western Meseta, Morocco: paleogeographic implications and interpretation of AFT age discrepancies. Tectonophysics 475, 29–37.
Sandoval, J., O'Dogherty, L., Guex, J., 2001. Evolutionary rates of Jurassic ammonites in relation to sea-level fluctuations. Palaios 16, 311–335.
Sass, E., Bein, A., Almogilabin, A., 1991. Oxygen-isotope composition of diagenetic calcite in organic-rich rocks – evidence for O-18 depletion in marine anaerobic pore water. Geology 19, 839–842.
Schlager, W., 1981. The paradox of drowned reefs and carbonate platforms. Geol. Soc. Am. Bull. 92, 197–211.
Schlager, W., 2003. Benthic carbonate factories of the Phanerozoic. Int. J. Earth Sci. 92, 445–464.
Scotese, C.R., 2016. In: Project, P. (Ed.), PALEOMAP PaleoAtlas for GPlates and the PaleoData Plotter Program.
Septfontaine, M., 1985. Milieux de dépôts et foraminifères (Lituolidés) de la plate-forme carbonatée du Lias moyen au Maroc. Rev. Micropaleontol. 28, 265–289.
Souhel, A., 1996. Le Mésozoïque dans le Haut-Atlas de Beni-Mellal(Maroc): stratigraphie, sédimentologie et évolution géodynamique. Laboratoire de géologie sédimentaire et paléontologie. Université Paul Sabatier, Toulouse.
Souhel, A., El Hariri, K., Chafiki, D., Canerot, J., 1998. Stratigraphie séquentielle et évolution géodynamique du Lias (Sinémurien terminal - Toarcien moyen) de l'Atlas de Béni-Mellal (Haut Atlas central, Maroc); Liassic (uppermost Sinemurian up to mid Toarcian) sequence stratigraphy and geodynamic evolution of the Beni-Mellal Atlas (Central High Atlas, Morocco). Bull. Soc. Geol. France 169, 527–536.
Soussi, M., Ben Ismail, M.H., 2000. Platform collapse and pelagic seamount facies: Jurassic development of Central Tunisia. Sediment. Geol. 133, 93–113.
Storm, M.S., Hesselbo, S.P., Jenkyns, H.C., Ruhl, M., Ullmann, C.V., Xu, W., Leng, M.J., Riding, J.B., Gorbanenko, O., 2020. Orbital pacing and secular evolution of the Early Jurassic carbon cycle. Proc. Natl. Acad. Sci. 117, 3974.
Stüder, M., du Dresnay, R., 1980. Déformations synsedimentaires en compression pendant le Lias superieur et le Dogger, au Tizi n'Irhil (Haut Atlas central de Midelt, Maroc). Bulletin de la Société géologique de France S7-XXIIpp. 391–397.
Suan, G., Mattioli, E., Pittet, B., Mailliot, S., Lecuyer, C., 2008. Evidence for major environmental perturbation prior to and during the Toarcian (Early Jurassic) oceanic anoxic event from the Lusitanian Basin, Portugal. Paleoceanography 23.
Suan, G., Mattioli, E., Pittet, B., Lecuyer, C., Sucheras-Marx, B., Duarte, L.V., Philippe, M., Reggiani, L., Martineau, F., 2010. Secular environmental precursors to Early Toarcian (Jurassic) extreme climate changes. Earth Planet. Sci. Lett. 290, 448–458.
Suan, G., Nikitenko, B.L., Rogov, M.A., Baudin, F., Spangenberg, J.E., Knyazev, V.G.,

Glinskikh, L.A., Goryacheva, A.A., Adatte, T., Riding, J.B., Föllmi, K.B., Pittet, B., Mattioli, E., Lecuyer, C., 2011. Polar record of Early Jurassic massive carbon injection. Earth Planet. Sci. Lett. 312, 102–113.
Suan, G., Schlögl, J., Mattioli, E., 2016. Bio- and chemostratigraphy of the Toarcian organic-rich deposits of some key successions of the Alpine Tethys. Newsl. Stratigr. 49, 401–419.
Suchéras-Marx, B., Mattioli, E., Allemand, P., Giraud, F., Pittet, B., Plancq, J., Escarguel, G., 2019. The colonization of the oceans by calcifying pelagic algae. Biogeosciences 16, 2501–2510.
Sumner, D.Y., Grotzinger, J.P., 1993. Numerical modeling of ooid size and the problem of neoproterozoic giant ooids. J. Sediment. Petrol. 63, 974–982.
Svensen, H., Planke, S., Chevallier, L., Malthe-Sorenssen, A., Corfu, F., Jamtveit, B., 2007. Hydrothermal venting of greenhouse gases triggering Early Jurassic global warming. Earth Planet. Sci. Lett. 256, 554–566.
Svensen, H.H., Torsvik, T.H., Callegaro, S., Augland, L., Heimdal, T.H., Jerram, D.A., Planke, S., Pereira, E., 2018. Gondwana Large Igneous Provinces: plate reconstructions, volcanic basins and sill volumes. Geol. Soc. Lond., Spec. Publ. 463, 17.
Teixell, A., Arboleya, M.L., Julivert, M., Charroud, M., 2003. Tectonic shortening and topography in the central High Atlas (Morocco). Tectonics 22.
Them, T.R., Gill, B.C., Caruthers, A.H., Gröcke, D.R., Tulsky, E.T., Martindale, R.C., Poulton, T.P., Smith, P.L., 2017a. High-resolution carbon isotope records of the Toarcian Oceanic Anoxic Event (Early Jurassic) from North America and implications for the global drivers of the Toarcian carbon cycle. Earth Planet. Sci. Lett. 459, 118–126.
Them, T.R., Gill, B.C., Selby, D., Gröcke, D.R., Friedman, R.M., Owens, J.D., 2017b. Evidence for rapid weathering response to climatic warming during the Toarcian Oceanic Anoxic Event. Sci. Rep. 7, 5003.
Them, T.R., Gill, B.C., Caruthers, A.H., Gerhardt, A.M., Grocke, D.R., Lyons, T.W., Marroquin, S.M., Nielsen, S.G., Alexandre, J.P.T., Owens, J.D., 2018. Thallium isotopes reveal protracted anoxia during the Toarcian (Early Jurassic) associated with volcanism, carbon burial, and mass extinction. Proc. Natl. Acad. Sci. U. S. A. 115, 6596–6601.
Them, T.R., Jagoe, C.H., Caruthers, A.H., Gill, B.C., Grasby, S.E., Gröcke, D.R., Yin, R., Owens, J.D., 2019. Terrestrial sources as the primary delivery mechanism of mercury to the oceans across the Toarcian Oceanic Anoxic Event (Early Jurassic). Earth Planet. Sci. Lett. 507, 62–72.
Trecalli, A., Spangenberg, J., Adatte, T., Föllmi, K.B., Parente, M., 2012. Carbonate platform evidence of ocean acidification at the onset of the early Toarcian oceanic anoxic event. Earth Planet. Sci. Lett. 357, 214–225.
Tribovillard, N., Algeo, T.J., Lyons, T., Riboulleau, A., 2006. Trace metals as paleoredox and paleoproductivity proxies: an update. Chem. Geol. 232, 12–32.
Trower, E.J., Lamb, M.P., Fischer, W.W., 2017. Experimental evidence that ooid size reflects a dynamic equilibrium between rapid precipitation and abrasion rates. Earth Planet. Sci. Lett. 468, 112–118.
Ullmann, C.V., Thibault, N., Ruhl, M., Hesselbo, S.P., Korte, C., 2014. Effect of a Jurassic oceanic anoxic event on belemnite ecology and evolution. Proc. Natl. Acad. Sci. U. S. A. 111, 10073–10076.
Ullmann, C.V., Boyle, R., Duarte, L.V., Hesselbo, S.P., Kasemann, S.A., Klein, T., Lenton, T.M., Piazza, V., Aberhan, M., 2020. Warm afterglow from the Toarcian Oceanic Anoxic Event drives the success of deep-adapted brachiopods. Sci. Rep. 10, 6549.
Vasseur, R.l., 2018. Extinctions et recouvrements de coraux au cours de la crise Pliensbachien - Toarcien.
Weedon, G.P., Jenkyns, H.C., 2003. Evidence for rapid climate change in the Mesozoic-Palaeogene greenhouse world - Discussion. Philos. Trans. R. Soc. Lond. Ser. A Math. Phys. Eng. Sci. 361 1916.
Weissert, H., 2000. Global change – deciphering methane's fingerprint. Nature 406, 356–357.
Wignall, P.B., Newton, R.J., Little, C.T.S., 2005. The timing of paleoenvironmental change and cause-and-effect relationships during the early Jurassic mass extinction in Europe. Am. J. Sci. 305, 1014–1032.
Wilmsen, M., Neuweiler, F., 2008. Biosedimentology of the Early Jurassic post-extinction carbonate depositional system, central High Atlas rift basin, Morocco. Sedimentology 55, 773–807.
Wilmsen, M., Blau, J., Meister, C., Mehdi, M., Neuweiler, F., 2002. Early Jurassic (Sinemurian to Toarcian) ammonites from the central High Atlas (Morocco) between Er-Rachidia and Rich. Rev. Paléobiol. 21, 149–175.
Xu, Ruhl, Jenkyns, Leng, Huggett, Minisini, Ullmann, Riding, Weijers, Storm, Percival, Tosca, Idiz, Tegelaar, Hesselbo, 2018. Evolution of the Toarcian (Early Jurassic) carbon-cycle and global climatic controls on local sedimentary processes (Cardigan Bay Basin, UK). Earth Planet Sc Lett 484, 396–411.